DEVELOPMENTAL AND EVOLUTIONARY COMPARATIVE ANALYSIS OF A *HOXD* REGULATORY LANDSCAPE IN MAMMALS AND BIRDS

Aurélie Hintermann[1], Isabel Guerreiro[1,a], Christopher Chase Bolt[2], Sandra Gitto[1], Denis Duboule[1,2,3,#] and Leonardo Beccari[1,b]

Short title: Evolution of long-range regulation at the *HoxD* locus

Keywords: Chromatin topology, TAD, enhancers, evolution, gene regulation, development, teguments, placodes

[1]Department of Genetics and Evolution, University of Geneva, 30 quai Ernest-Ansermet, 1211, Geneva, Switzerland.
[2]School of Life Sciences, Federal School of Technology (EPFL), 1015 Lausanne, Switzerland.
[3]Collège de France, 75005 Paris, France.

[a]Present address: Oncode Institute, Hubrecht Institute-KNAW and University Medical Center Utrecht, Utrecht, The Netherlands.

[b]Present address: Institut Neuromyogène. CNRS UMR 5310, INSERM U1217, University of Lyon, Lyon, France.

[#]Corresponding author

Denis Duboule
Denis.Duboule@unige.ch

ABSTRACT

Modifications in gene regulation during development are considered to be a driving force in the evolution of organisms. Part of these changes involve rapidly evolving *cis*-regulatory elements (CREs), which interact with their target genes through higher-order 3D chromatin structures. How such 3D architectures and variations in CREs contribute to transcriptional evolvability nevertheless remains elusive. During vertebrate evolution, *Hox* genes were redeployed in different organs in a class-specific manner, while maintaining the same basic function in organizing the primary body axis. Since a large part of the relevant enhancers are located in a conserved regulatory landscape, this gene cluster represents an interesting paradigm to study the emergence of regulatory innovations. In this work, we analyzed *Hoxd* gene regulation in both murine vibrissae and chicken feather primordia, two mammalian- and avian-specific skin appendages which express different subsets of *Hoxd* genes, and compared their regulatory modalities with the regulations at work during the elongation of the posterior trunk, a mechanism highly conserved in amniotes. We show that in the former two structures, distinct subsets of *Hoxd* genes are contacted by different lineage-specific enhancers, likely as a result of using an ancestral chromatin topology as an evolutionary playground, whereas the regulations implemented in the mouse and chicken embryonic trunk rely more on conserved CREs. Nevertheless, a high proportion of these non-coding sequences active in the trunk appear to have functionally diverged between the two species, suggesting that transcriptional robustness is maintained despite a considerable divergence in CREs' sequence, an observation supported by a genome-wide comparative approach.

INTRODUCTION

Changes in the spatial and temporal regulation of genes critical for developmental processes have greatly contributed to the evolution of animal morphologies (see for example (Carroll, 2008; Rebeiz et al., 2015). The expression of such genes is generally modulated by combinations of *cis*-regulatory elements (CREs), short DNA sequences enriched for transcription factor binding sites, which tend to evolve more rapidly than the genes they control (Edwards et al., 2013; Long et al., 2016; Spitz and Furlong, 2012). CREs can be spread over large distances around the gene(s) they regulate, which gives to the spatial organization of chromatin a particular importance. Indeed, the existence of such 'regulatory landscapes' (Spitz et al., 2003) implies that enhancer-promoter interactions involve spatial proximity, which is generally thought to occur through large chromatin loops (Rao et al., 2014).

Regulatory landscapes often correspond to Topologically Associating Domains (TADs) (Andrey et al., 2013; Harmston et al., 2017), which were defined as chromatin domains where the probabilities of interactions, as measured by chromosome conformation capture (Belton et al., 2012), are higher when compared to the neighbouring regions (Dixon et al., 2016, 2012; Nora et al., 2012). The distribution of TADs tends to be conserved in various vertebrate species, a phenomenon likely associated with regulatory constraints exerted by the complex and pleiotropic regulations found around many vertebrate developmental genes. Such domains, where many interactions might occur, were proposed to form particular chromatin niches, rich in various DNA-binding proteins where the evolutionary emergence of novel regulatory sequences could be favoured due to the presence of both a pre-existing scaffold and appropriate co-factors. While genomic rearrangements altering the structure of TADs were reported to impact proper gene regulation during development leading to genetic syndromes (e.g. (Bolt et al., 2021; Lupiáñez et al., 2015), in most cases, these rearrangements also affected enhancer-promoter spatial relationships, which makes a causal assessment difficult.

Genome-wide analyses carried out in different species, comparing DNA sequence conservation, TAD organization, or some epigenetic modifications, have started to reveal some of the molecular mechanisms underlying both the evolution of gene regulation and, by extension, the modification of species-specific traits. However, integrated functional approaches are required to better understand how changes in chromatin architecture and modifications in CREs may contribute to this evolutionary process, in particular how these parameters can influence the evolvability and the robustness of gene transcription. To try to address such questions, we have used the *HoxD* locus as a paradigm of pleiotropic regulation of a multi-gene family, with a strong impact both on the control of important developmental steps, and on the emergence of evolutionary novelties.

The *HoxD* cluster contains a series of *Hoxd* genes in *cis*, which encode transcription factors that are expressed in different combinations across several embryonic structures. The cluster is flanked by two large TADs, each one matching a gene desert highly enriched in CREs (Darbellay and Duboule, 2016). These two TADs are separated by a boundary region rich in CTCF binding sites which is localized within the cluster,

close to its centromeric extremity (Andrey et al., 2013; Rodriguez-Carballo et al., 2017). The telomeric TAD comprises a large number of enhancers controlling transcription of various *Hoxd* genes in most of the tissues where HOX proteins operate (Andrey et al., 2013; Darbellay et al., 2019; Delpretti et al., 2013; Guerreiro et al., 2016; Schep et al., 2016). In contrast, the centromeric TAD contains enhancers specific for terminal structures such as digits or external genitals (Amândio et al., 2020; Montavon et al., 2011).

Amongst the many tissues where *Hoxd* genes exert a function are embryonic primordia of different dermal condensations including those of mammary glands, vibrissae and pelage hairs of mammals and those of chicken feathers (Kanzler et al., 1997, 1994; Reid and Gaunt, 2002; Reynolds et al., 1995; Schep et al., 2016)(Fig. 1). Despite the fact that these ectodermal structures share common developmental mechanisms and gene regulatory networks such as the *Wnt*, EDA and BMP signaling pathways (Biggs and Mikkola, 2014; Dhouailly et al., 2019; Di-Poï and Milinkovitch, 2016; Pantalacci et al., 2008; Wu et al., 2004), each type of primordium expresses different subsets of contiguous *Hoxd* genes, suggesting that they were co-opted in these structures following slightly different mechanisms or, alternatively, that their regulations subsequently diverged in each lineage. Since the specific topological organization of the *HoxD* locus is present in fishes (Acemel et al., 2016), it predates the emergence of hairs and feathers during amniote evolution (Dhouailly, 2009; Wu et al., 2004). For this reason, these organs represent valuable models to understand how CRE evolution within a pre-existing chromatin architecture could lead to the implementation of new gene-specific expression patterns. In contrast, the general organization of *Hoxd* gene expression along the main embryonic body axis is overall maintained across vertebrates species, in spite of the low sequence conservation observed, raising the question as to how evolving *Hox* clusters could maintain globally similar transcriptional outputs.

In this study, we try to address these issues by taking a comparative look at a well-defined regulatory landscape, positioned telomeric to the *HoxD* gene cluster, in mammals and in birds, i.e. two syntenic regions containing CREs involved either in the same regulatory tasks, or controlling regulatory aspects specific to each taxon. In the latter context, we characterized *Hoxd* gene regulation in the mouse-specific vibrissae primordia (VPs) and in the chicken-specific feather primordia (FPs). We show that different subsets of contiguous *Hoxd* genes are expressed in the mouse VP mesoderm and in the chicken FP ectoderm, indicating an independent co-option of *Hoxd* paralogs in these structures. While the transcription of these genes in VPs and FPs relies on different sets of lineage-specific CREs, located within different *Hoxd* interacting regions, these CREs exploit a largely constitutive chromatin 3D architecture.

Our comparative analysis of the regulation at work during trunk extension also revealed that *Hoxd1* displays an expression pattern markedly different from that of its neighboring paralogs, both in mouse and chick, and that this *Hoxd1*-specific expression is driven by an evolutionary conserved CRE located in a region predominantly interacting with *Hoxd1* in both species. However, the cis-regulatory code at work in the latter regulation strongly differs between the two species, illustrating the possibility that inter-species conservation of both gene transcriptional specificity and chromatin architectures are compatible with a high plasticity of the *cis*-regulatory sequences involved. The extension of this observation genome-wide suggests that conserved CRE sequences more frequently diverge in their regulatory activity rather than maintaining their functionality.

RESULTS

Divergent *Hoxd* gene regulation in mammalian and avian skin appendages.

We initially analyzed the expression profiles of *Hoxd* genes in mouse VPs and chicken FPs (Fig. 1). Skin appendage development starts with the interaction of the skin ectoderm with its underlying mesoderm, resulting in the thickening of the epithelium into a placode and in the condensation of dermal cells into a papilla (Mikkola, 2007; Sawyer and Knapp, 2003; Widelitz and Chuong, 1999). Mammalian VPs start developing at early embryonic day 12 (E12), forming a stereotyped array of eight columns and five rows of VPs (Wrenn and Wessells, 1984)(Fig. 1A). The epithelial placode subsequently invaginates and engulfs the dermal papilla forming the follicle primordium (Fig. S1). Likewise, in birds, ectoderm-mesoderm interactions result in the evagination of feather buds around embryonic day 7 (stage HH30-32 (Hamburger and Hamilton, 1951; Michon et al., 2007) (Fig. S2). Whole-mount *in situ* hybridization (WISH) revealed strong *Hoxd1* expression in the dermal papillae of the VPs (Fig. 1B; Fig. S1B). Furthermore, a comparative analysis of VPs from single E12.5 embryos revealed that *Hoxd1* transcripts accumulate slightly after ectodermal placode formation, marked by the expression of *Shh* (Chiang et al., 1999) (Fig. S1C).

Both *Hoxd3* and *Hoxd4* are also expressed in VPs, but at much lower levels than *Hoxd1* (Fig. 1B, Fig. S1E) and faint levels of *Hoxd8* mRNAs were sporadically detected in the VPs, while *Hoxd9* and more 5'-located *Hoxd* mRNAs were never observed in these structures (Fig. 1B, Fig. S1E). *In situ* hybridization on cryostat sections confirmed that *Hoxd1* transcripts accumulate in the dermal mesenchyme of VPs, but not in the ectoderm-derived portion of the follicle (Fig. S1B). Therefore, *Hoxd1-Hoxd4* are transcriptionally active in the dermal papillae of developing VPs, with *Hoxd1* being the main paralog expressed in this structure.WISH experiments in HH35 chicken embryos revealed expression of *HOXD3*, *HOXD4, HOXD8* and *HOXD9* in the FPs, while *HOXD1* and *HOXD11* mRNAs were not detected (Fig. 1C, D, Fig S2). Cryostat sections indicated that *HOXD* gene expression in chicken FPs is localized in the follicle ectoderm (Fig. S2B), in contrast with murine VPs. Different *Hoxd* genes thus operate in dermal papillae of mouse VPs and in ectodermal placodes of chicken FPs, likely reflecting the implementation of different regulatory mechanisms in the two lineages.

Hoxd gene regulation in the mouse and chicken embryonic body axis.

Hox genes are expressed in the paraxial and lateral mesoderm of the main embryonic axis, as well as in the neural tube, and display a progressively more restricted expression domain depending on their position within the cluster (Gaunt, 1988). Comparative WISH analysis of mouse and chicken embryos revealed that *Hoxd1* expression patterns in the trunk were markedly similar between the two species, yet largely divergent from that of the 5'-located neighbour *Hoxd* paralogs (Fig. 1E-G). While *Hoxd3-Hoxd8* were strongly and uniformly transcribed in the mouse paraxial and lateral mesoderm as well as in the neural tube, *Hoxd1* displayed a biphasic expression pattern. Transcripts accumulated in the embryonic tailbud, yet they rapidly disappeared from the presomitic mesoderm and remained undetected in lateral mesoderm progenitors or in the neural tube (Fig. 1F). Instead, *Hoxd1* was specifically re-activated during somite condensation, coupling the transcription of this gene to the somitogenesis clock (Dale and Pourquié, 2000; Zákány et al., 2001). Similar to the mouse pattern, the chicken *HOXD1* expression also differed from its neighboring paralogs, even though

its transcripts remained detectable in the formed somites all along the main body axis (Fig. 1G). These observations suggested that *Hoxd1* transcription in developing somites may depend on a specific set of CREs, different from CREs controlling the neighboring paralogs, and that this locus-specific regulation was evolutionarily conserved across amniotes.

Conserved paralogous regulatory landscapes.

In order to see whether these differences and similarities in regulatory specificities could be associated to variations in the global chromatin architectures at the gene cluster and the flanking telomeric TAD, we performed Capture HiC (CHiC) experiments using dissected mouse and chicken posterior trunks (Fig. 2A, B). Even though the general TAD organization at this locus is approximately two times smaller in the chicken genome, the *HOXD* region closely resembled its mouse counterpart, with the T-DOM being further organized into two sub-TADs in both species (Fig. 2, sub-TAD1 and sub-TAD2) (Rodríguez-Carballo et al., 2020; Yakushiji-Kaminatsui et al., 2018). Of note, both the presence and distribution of conserved non-coding elements (CNEs) was maintained within this similar chromatin architecture (Fig. 2, Fig. S3A).

We corroborated these observations by assessing the interactions established by the *Hoxd1*, *Hoxd4* and *Hoxd9* promoters in mouse and chicken embryonic posterior trunk cells, using 4C-seq (Fig. S3). As a reference for constitutive interactions, we used embryonic brains where *Hox* genes are not transcribed. In both species, all three viewpoints contacted sub-TAD1 with a higher probability than sub-TAD2, showing specific and non-overlapping regions where interactions were enriched. *Hoxd1* contacted the first half of sub-TAD1 (Fig. S3, D1) more intensively than *Hoxd4* or *Hoxd9.* In turn, *Hoxd4* contacts within the 3' half of *HoxD* sub-TAD1 were increased up to the sub-TAD boundary (Fig. S3, D4). Finally, *Hoxd9* interactions were mostly limited to the sub-TAD boundary region (Fig. S3, D9), where they were higher than for *Hoxd4*. These preferentially interacting regions within the 3' TAD were found in both brain and posterior trunk cells, yet with an overall lower contact frequency in the brain, reflecting the default and transcription-independent conformation of the region, as shown in (Andrey et al., 2013; Dekker and Heard, 2015; Noordermeer et al., 2011).

Chromatin architectures largely rely upon the zinc-finger protein CTCF which, together with the cohesin complex, can induce the formation and stabilisation of large loops. (Hansen et al., 2017; Nanni et al., 2020; Pugacheva et al., 2020). The ChIP-seq analysis of the CTCF profiles revealed that both at the mouse and chicken *HoxD* loci, a bound CTCF site is observed between the D1 and D4 regions (Fig. S3, blue arrowhead). Also, as previously reported (Rodriguez-Carballo et al., 2017; Rodríguez-Carballo et al., 2020; Yakushiji-Kaminatsui et al., 2018), a cluster of CTCF binding sites delimits the boundary between the mouse and the chicken sub-TAD1 and sub-TAD2, thus making the transition between the D4 and D9 regions in both species (Fig. 2; Fig. S3). These results suggest that the evolutionarily conserved contact topology of 3' *Hoxd* genes within the T-DOM may contribute to the specific expression of *Hoxd1* in mouse and chicken embryonic structures.

Searching for similar and divergent inter-species regulatory sequences.

To identify potential regulatory sequences within those regions showing preferential interactions with *Hoxd* target genes in either the VPs, the FPs and in posterior trunk cells, we carried out ChIP-seq analyses

using an antibody against H3K27ac, a histone modification indicative of an active chromatin state (Creyghton et al., 2010; Rada-Iglesias et al., 2011). The profile of H3K27ac in fetal brains was used as a negative control to identify putative tissue-specific CREs after microdissections of a comparable piece of fetal skin containing the primordia of either VPs or FPs. In all H3K27ac profiles, the T-DOM contained most of the tissue-specific enrichment, whereas H3K27ac signals over the C-DOM were virtually absent (Fig. 3).

We identified those genomic regions residing outside of genes and promoters and accounting for the highest tissue-specific H3K27ac enrichment (hereafter referred to as Most Acetylated Regions, MARs; see materials and methods). We annotated the MARs of both the mouse VPs and the chicken FPs (Fig. 3, red rectangles) and compared them to the extent of the regions preferentially interacting with *Hoxd1*, *Hoxd4* and *Hoxd9* promoters (D1, D4 and D9 respectively)(Fig. 3). In the mouse VPs, the MARs mostly mapped within the D1 region (8 tissue-specific H3K27ac -positive elements)(Fig. 3A; Fig. S4A), in agreement with the relatively stronger expression of *Hoxd1* there, when compared to its neighbors (Fig. 1B; Fig. S1D). Instead, in chicken dorsal skin samples, where *HOXD1* is not active (Fig. 1D), only two H3K27ac-positive sequences were located within the D1 region and the MARs largely overlapped the D4-D9 interacting region (Fig. 3A, red rectangle; Fig. S4A). Therefore, VPs and FPs display different distributions of H3K27ac-positive elements across the T-DOM, in agreement with the specific *Hoxd* gene subsets that are expressed in these tissues. In contrast, the MARs of mouse and chicken PT samples both overlapped the D4 region (Fig. 3B, red rectangles; Fig. S4B). This result is in agreement with the similar expression patterns in the embryonic trunk of the two species, and with the domain of expression of *Hoxd4* being more extended than that of *Hoxd9*. Of note, different H3K27ac-positive elements were identified within the mouse and chicken D1 region, suggesting that they could contribute to the specific transcription of *Hoxd1* in the developing somites.

Eutherian-specific elements controlling *Hoxd1* in the vibrissae progenitors.

We further characterized the interactions between the *Hoxd1, Hoxd4* and *Hoxd9* promoters with the D1 region by performing 4C-seq analyses in microdissected E12.5 VPs (Fig. S5A, orange profiles), using brain cells as a negative control (Fig. S5A, grey profiles, overlaps in braun). We observed that, while the interactions established by the active *Hoxd1* gene increased specifically within region D1 in the VP sample when compared to the brain, *Hoxd4* displayed only a modest augmentation of contacts in the same region and the interactions with *Hoxd9* remained essentially the same in both tissues (Fig. S5A), as expected from these latter two genes, which are not transcribed in the VPs. In contrast, when the profiles obtained from posterior trunk cells, where both *Hoxd4* and *Hoxd9* are active, were subtracted from the VP profiles, a gain of both *Hoxd4* and *Hoxd9* reads were observed in their respective binding D4 and D9 regions (Fig. S5A, dark braun profiles inbetween the 4C profiles). Indeed, gained signals for the *Hoxd4* viewpoint were mostly scored over the D4 region whereas the D9 region was enriched in contacts established by *Hoxd9* (Fig. S5A).

We then analyzed *Hoxd1* expression in the VPs of mouse embryos carrying different deletions of the T-DOM (Fig. 4A, B). In the $HoxD^{Del(AttP\text{-}TpSB2)lac}$ allele, a 150kb large piece of DNA directly adjacent to the *HoxD* cluster was removed (hereafter referred to as Del(Attp-SB2). Since Del(Attp-SB2) homozygous embryos are not viable due to the deletion of the essential *Mtx2* gene (Andrey et al., 2013), we crossed this line with the mouse line $HoxD^{Del(1\text{-}13)d9Lac}$ (Spitz et al., 2001) hereafter referred to as Del(1-13). In this line, the

entire *HoxD* cluster is replaced by a *Hoxd9::LacZ* transgenic cassette (Fig. 4C), such as to be able to see the effect of the $HoxD^{Del(AttP\text{-}SB2)lac}$ deletion upon *Hoxd* gene regulation *in cis*. As expected, *Hoxd1* and *Hoxd4* expression in the VPs of trans-heterozygous $HoxD^{Del(AttP\text{-}TpSB2)Lac/Del(1\text{-}13)}$ mutant embryos was completely abolished, in contrast with Del(1-13) heterozygous control littermates. Conversely, the $HoxD^{Del(TpSB2\text{-}TpSB3)lac}$ allele (hereafter Del(SB2-SB3)(Andrey et al., 2013) carries a large deletion spanning the second half of sub-TAD1 and the entire sub-TAD2. We detected robust *Hoxd1* expression in the VPs of E12.5 Del(SB2-SB3) homozygous mutant embryos (Fig. 4A).

We complemented these results by producing mouse transgenic embryos carrying bacterial artificial chromosomes (BACs) spanning the *HoxD* cluster and/or parts of sub-TAD1 (Fig. 4C). In agreement with the analysis of the T-DOM deletions, the BACs covering either the *HoxD* cluster (BAC^{HoxD} (Schep et al., 2016) or mapping outside of the Attp-SB2 region (BAC^{T1} (Delpretti et al., 2013) did not display any LacZ reporter activity in E12.5 to E13.5 VPs. Instead, mouse embryos transgenic for BAC^{Mtx2} (Allais-Bonnet et al., 2021), which covers most of the Attp-SB2 region (and corresponds closely with the D1 region), displayed strong reporter expression in the VPs (Fig. 4B). These results demonstrate that the Attp-SB2 region is both necessary and sufficient to drive *Hoxd* gene expression in the developing VPs.

Together with the WISH and 4C-seq data, these results delimited a segment of 148kb hereafter referred to as the VP regulatory region (Fig. 4C, VPRR), a region that closely overlaps with VP-specific MAR region (Fig. 3A). In particular, the comparison between the H3K27ac profiles in E12.5 VPs and brain cells identified at least four non-coding sequences (or groups thereof-) located within the VPRR and referred to as VP acetylated elements (VPAEs)(Fig. 4D, open arrowheads). Phylogenetic footprinting analysis revealed that all four elements are conserved across Therians, which include placental mammals and marsupials (Fig. S5B). Noteworthy, a core VPAE3 sequence is also conserved in reptiles and birds, suggesting that this sequence evolved earlier in the tetrapod lineage. To assess the regulatory potential of these sequences, we cloned small regions containing the four VPAEs into a *LacZ* reporter vector upstream of the *ß-globin* minimal promoter and tested them in transient transgenic assays (Fig. 4D, tgVPAE1-4; Fig. S5C). Amongst the tested CREs, VPAE2 displayed strong and reproducible enhancer activity in VPs (Fig. 4E), comparable to that observed in embryos transgenic for BAC^{Mtx2}. Instead, ß-galactosidase activity in VPs was not scored for VPAE1, VPAE3, or VPAE4 transgenic embryos (Fig. S5C). These results indicated that the expression of *Hoxd1* to *Hoxd4* in VPs depends at least on the VPAE2 enhancer, located 120 kb 3' to the *Hoxd1* transcription start site within the D1 region. Noteworthy, in Del(Attp-SB2) mouse embryos, expression of *Hoxd1* was also abolished from facial mesenchymal progenitors, suggesting that this regulatory region includes other CREs controlling this gene.

Lineage-specific regulatory sequences in chicken feather buds.

We also examined the evolutionary conservation of non-coding elements specifically enriched in H3K27ac marks in micro-dissected dorsal skin samples of chick embryos and located within the MARs-containing region defined for this structure (Fig. 3A). While the vast majority of these elements could not be identified in mammals (Fig. S6), they were found conserved across birds and reptiles indicating a lineage-specific evolution of CREs driving *Hoxd* gene expression in FPs, analogous to what was observed for the mouse VPs. These results further support the idea that the evolutionary emergence of lineage-specific CREs

within an ancestral chromatin topology may have triggered differential *Hoxd* gene regulation in mammalian and avian skin appendages.

Tetrapod-conserved regulatory elements active in forming somites.

The expression of *Hoxd1* during the extension of the mouse and chicken embryonic axes differs substantially from that of the neighboring *Hoxd* genes (Fig. 1B, D; Fig. S1E). We could thus expect that the accompanying regulations might involve *Hoxd1*-specific interacting elements, distinct from the MARs identified for the mouse and chicken embryonic PTs (Figs. 3B and S4B). To try to localize the CRE(s) active over *Hoxd1* in forming somites, we initially looked at different alleles where deletions had been engineered (Fig. 4F, G). *Hoxd1* expression was abolished in developing somites of Del(Attp-SB2) E9.5 embryos, compared to their control Del(1-13) littermates (Fig. 4F), while similar transcript levels were maintained in the tailbuds, suggesting that *Hoxd1* regulation in both structures involves different regulatory sequences. Accordingly, embryos transgenic for BAC^{Mtx2} displayed strong LacZ staining in somites but not in the tailbud, with stronger activity in the last formed somites, thus closely mimicking *Hoxd1* transcription in these structures (Zákány et al., 2001). In contrast, *LacZ* expression was uniform along the paraxial mesoderm of TgBAC^{HoxD} transgenic embryos, yet without showing any *Hoxd1*-like specific reporter activity in the forming somites (Fig. 4G).

The H3K27ac profiles revealed that most of the signals specific for posterior trunk cells (SAEs) were located in the D4 sub-region, a region involved in *Hoxd* gene regulation in paraxial and lateral plate mesoderm derivatives (Fig. 4G, tgBAC^{T1}). Amongst those H3K27ac peaks mapping within the genomic interval spanned by the Del(Attp-SB2) mutation and covered by BAC^{Mtx2} , two were assessed by transgenic analysis (Fig. 4H; black arrowheads). While the SAE sequence within VPAE3, conserved throughout tetrapods, gave expression in the forming somites (Fig. 4I), the other SAE sequence, which was not conserved except in Eutherians, did not show any signal in these structures (Fig. S5B, D). The chicken sequence orthologous to mouse VPAE3 was also found enriched in H3K27ac in chicken posterior trunk cells (Fig. S4B), suggesting that it is functionally conserved in mammals and birds. These results indicated that the regulation of *Hoxd1* in the forming somites depends on a specific set of enhancers, which are in part conserved across amniotes and differ from those controlling other *Hoxd* genes in the paraxial and lateral mesoderm.

Conservation and divergence of *HoxD* enhancers in mouse and chicken embryonic trunk cells.

When mouse VP and dorsal chicken skin were used, the H3K27ac profiles revealed that the vast majority of H3K27ac-positive elements are not conserved between the two species. This is in contrast with posterior embryonic trunk cells, where the proportion of H3K27ac-positive elements coinciding with a conserved sequence was considerably higher. Surprisingly, however, several conserved elements enriched in H3K27ac in either the mouse or the chicken posterior trunk cells, were not enriched in the same tissue of the other species (Fig. S4), illustrating a divergence in the combinations of CREs at work in this dissected piece of embryonic tissue, in contrast with the otherwise well-conserved chromatin architectures and expression patterns.

We next wanted to assess whether this discrepancy between the inter-species sequence conservation on the one hand, and their H3K27ac coverage in the same developing tissues on the other hand, would also

occur outside the *HoxD* locus. We compared H3K27ac profiles across different tissues (proximal and distal forelimb buds, fetal skin, brain and posterior trunks) of mouse and chicken embryos genome-wide and related them to sequence conservation. In both mouse and chicken, the majority of non-coding H3K27ac-positive elements mapping more than 2kb away from a gene transcription start site (putative enhancers, hereafter referred to as enhancers) displayed H3K27ac enrichment in only one or the other of the embryonic structures analyzed (Fig. 5A). Instead, most H3K27ac-positive elements located less than 2kb far from the transcription start sites ('promoters') were enriched across different samples (Fig. 5A), a result in agreement with the generally pleiotropic expression of genes with important developmental functions. However, the proportion of enhancers displaying H3K27ac in more than one tissue was significantly increased when considering only non-coding sequences which were evolutionary conserved between mouse and chicken (Fig. 5A; p-value < e-15, Fisher test).

In agreement with what was observed at the *HoxD* locus, the majority of enhancers evolutionarily conserved between mouse and chicken differed in their H3K27ac enrichment patterns between the two species (Fig. 5B, C). In fact, 79 percent (1141/1445) of the enhancers labelled by H3K27ac in only one of the embryonic tissues analyzed in chicken were either not active in any of the corresponding mouse samples, or active in different mouse embryonic structures. Accordingly, H3K27ac-positive enhancers scored in different chicken samples frequently diverged in their H3K27ac coverage when compared to the related mouse tissues (Fig. 5B). This data indicates that DNA sequence similarity between two species can be maintained in regulatory sequences despite divergences in their tissue-specific functionalities.

DISCUSSION

Versatile *Hoxd* gene functions in skin appendages.

Hox genes play a dual role in skin appendage development. While their colinear expression is initially necessary to pattern the skin dermis (Kanzler et al., 1997), they are subsequently transcribed in the dermal papillae and/or ectoderm of embryonic and adult hair pelage follicles and vibrissae precursors (Godwin and Capecchi, 1998; Packer et al., 2000; Reynolds et al., 1995; Yu et al., 2018), as well as in the avian buds (Chuong et al., 1990; Kanzler et al., 1997). Here we show that the dermal papillae of embryonic mouse vibrissae express *Hoxd1* to *Hoxd4*, with the former gene's mRNAs being the first detected, followed by considerably lower levels of *Hoxd3* and *Hoxd4* RNAs. The transcription in VPs is driven by CREs located in a region encompassing approximately 120kb of DNA adjacent to the telomeric end of the mouse *HoxD* cluster, a region that is preferentially contacted by the *Hoxd1* gene. Therefore, a proximity effect is observed in the building of a general chromatin architecture, based on constitutive contacts between the *Hoxd1* region and the neighbouring sub-TAD, whereby most of the *Hoxd1* regulatory sequences are located in the adjacent portion of the regulatory landscape.

While a detailed functional characterization of *Hoxd* genes during the development of whiskers was not the aim of this work, we did not observe any major morphological alteration in the vibrissae of mice carrying genetic deletions of this precise region, despite the complete abrogation in the expression of *Hoxd1* to *Hoxd4* in these structures. This lack of any visible abnormal phenotype may be due to functional redundancy

with other *Hox* paralogy groups expressed there, such as *Hoxc8* (Yu et al., 2018), to a lack of analytical power or of the appropriate behavioural paradigms that may have revealed abnormally function whiskers. The diverse expression of *Hox* paralogs in mammalian and avian skin appendages nonetheless illustrates the plasticity in the usage of *Hox* gene functions in these structures. This plasticity likely relies upon the independent acquisition of specific CREs for each gene cluster, as these skin derivatives emerged after the genome duplication events thought to be at the origin of the vertebrate lineage (Holland et al., 2008; Holland and Garcia-Fernàndez, 1996). This is also also supported by the observation that all VPAEs and FPAEs identified in this study are mammalian or avian specific.

While *Hoxd9, Hoxd11* and *Hoxd13* are expressed in the ectoderm-derived hair fibers (Godwin and Capecchi, 1998; Packer et al., 2000; Reynolds et al., 1995; Yu et al., 2018), we did not observe any *Hoxd1* in the vibrissae shaft, nor any LacZ activity when the TgBAC^{Mtx2} (carrying the VPRR) transgenics were used, indicating that these expression patterns may depend on different sets of CREs. Our data also show that the expression of *Hoxd3* to *Hoxd9* in the ectoderm of the chicken FPs depends on CREs unrelated to those operating in the mouse VPs. These observations may indicate that different sets of *Hoxd* genes were independently co-opted during the evolution of skin derivatives, likely through *de novo* enhancer acquisition in the mammalian and avian lineages, in a way related to the regulation of *Hoxd9 and Hoxc13* in the embryonic mammary buds and in the nails and hairs of mammals, respectively (Fernandez-Guerrero et al., 2020; Schep et al., 2016). Alternatively, the rapid pace of tegument evolution in tetrapods may have been accompanied by a divergence in enhancer sequences, which makes comparisons difficult. In this context, we can not rule out the possibility that *Hoxd* gene regulation in skin appendages of both mammals and birds derives from an initial pan-*Hoxd* expression pattern both in the ectoderm and mesoderm of skin appendages, which then evolved differently in each lineage through modification of the CRE complement located within the adjacent TAD. The fact that two CNEs acetylated in mouse VPs and chick FPs are also acetylated in mouse and chick posterior trunk cells may indicate that the former structures co-opted parts of the regulatory mechanisms at work in the latter. In this view, DNA sequence conservation may be due to constraints imposed by the function in the trunk rather than by the function in the skin.

Enhancer acquisition in evolving tetrapod skin appendages.

TADs which contain pleiotropic genes of key importance for development are frequently conserved across tetrapods and topological changes in their organization often correlate with important modifications in gene expression (Eres et al., 2019; Liao et al., 2021; Torosin et al., 2020; Yakushiji-Kaminatsui et al., 2018). Our results show that despite a considerable divergence in the non-coding elements localized in the mouse and chicken T-DOM, the global pattern of interactions is conserved leading to similar chromatin topologies. Indeed, in both cases, different *Hoxd* genes interact preferentially with distinct portions of sub-TAD1. These contacts are for the most constitutive, even though we observed an activity-dependent increase in interactions in the mouse VPs, and in mouse and chicken PT cells. Of interest, the regions within T-DOM, which were preferentially contacted by the *Hoxd1*, *Hoxd4* or *Hoxd9* genes (D1 to D9) are organized in a linear sequence opposite to the order of the genes themselves, as if *Hoxd1* was folding on its closest possible chromatin environment within T-DOM, bringing along *Hoxd3* towards the next chromatin segment and positioning the

interactions involving *Hoxd9* further away into T-DOM. This sequential positioning of interactions in mirror with spatial colinearity may impose a generic contact pattern, whereby *Hoxd9*, for example, is unable to establish strong interactions with the D1 region and its enhancers, for this region is primarily contacting *Hoxd1*, thus imposing constraints upon the distributions of interactions (see below).

Furthermore, the distribution of H3K27ac-positive regions in the chicken FPs and mouse VPs across these interacting regions correlated well with the specific subsets of *Hoxd* genes expressed in each of these tissues. Finally, the regulation of *Hoxd1* in developing somites relies on evolutionary conserved elements located in the region D1. This general regulatory topology is close to that observed in teleost fishes (Acemel et al., 2016; Woltering et al., 2014), suggesting that it was already in place at the root of the vertebrate lineage and that its hijacking by nascent enhancer sequences, may have favored the co-option of specific *Hoxd* gene subsets as targets of the novel regulations. The regulation of *Hoxd* genes in the mouse VPs and chicken FPs, as well in the mouse mammary buds (Schep et al., 2016) may illustrate this process.

Plasticity of the *cis*-regulatory code *versus* conservation in TAD organization.

Due to their functional relevance in the regulation of gene expression, CREs tend to be evolutionarily conserved across species (Sandelin et al., 2004; Sanges et al., 2013, 2006). However, several studies have shown that enhancers controlling developmental gene expression can be functionally conserved even across distant phylogenetic lineages despite a strong divergence in their DNA sequences (Ambrosino et al., 2019; Berthelot et al., 2018; Wong et al., 2020) (Eichenlaub and Ettwiller, 2011; Schmidt et al., 2010; Villar et al., 2015). Our inter-species comparison of CNEs enriched in H3K27ac across different embryonic structures revealed that a considerable portion of evolutionary conserved CREs diverged in their patterns of activity between the two species analyzed, in agreement with previous observations (Dermitzakis and Clark, 2002; Schmidt et al., 2010; Vierstra et al., 2014; Villar et al., 2015). This dichotomy between the conservation of enhancer sequences and their function is illustrated by the CREs controlling *Hoxd1* expression in the mouse and chicken developing somites. While some of the sequences active in the mouse posterior trunk are evolutionary and functionally conserved in chicken, such as VPAE3, which can drive LacZ expression in the last formed somites of the murine embryo, other elements conserved at the nucleotide level displayed H3K27ac enrichment only in the mouse.

In fact, a large fraction of H3K27ac-positive sequences detected either in the mouse or in the chicken PT cells were not conserved between the two species, suggesting that they evolved in a species-specific manner. In contrast, the high proportion of chicken promoters that display similar H3K27ac enrichments in mice, together with the similar expression patterns observed for mouse and chicken *Hoxd* genes in embryonic trunk cells, demonstrate that conserved gene expression can occur despite a high evolutionary plasticity in the *cis*-regulatory code usage, in agreement with previous reports (Berthelot et al., 2018; Snetkova et al., 2021). This may point to a regulatory strategy where multiple enhancers act coordinately to regulate the same target gene(s) thus creating a quantitive effect in a way similar to the reported action of super-enhancers (Sabari et al., 2018), yet where various subsets of CREs may display distinct tissue-specificities. This process may be implemented preferentially within large regulatory landscapes, as in the case of *Fgf8* (Marinic et al., 2013) or the TAD controlling *Hoxd* gene transcription in external genitals (Amândio et al., 2020).

A regulatory playground with constraints.

In those cases that were investigated, the respective positions of regulatory sequences within large syntenic regulatory landscapes are generally conserved, and the global regulatory architecture found at one particular developmental locus in one species can be extrapolated to its cognate locus in another amniote species (e.g. (Kragesteen et al., 2018), implying that enhancer-promoter interactions are also evolutionary well conserved, even for CREs acting over long distances (Irimia et al., 2012; Laverré et al., 2021), although some mechanistic elements may vary (Ushiki et al., 2021). In agreement with this, and contrasting with the apparent divergence in the *cis*-regulatory code controlling *Hoxd* gene expression in mouse and chicken embryos, our phylogenetic footprinting and epigenetic analysis revealed that non-coding elements conserved in their DNA sequence between the mouse and chicken genomes were distributed across the two species in a very similar manner. Therefore, the potential gain and/or loss in the two lineages of particular CREs did not significantly impact the internal organization of those conserved regulatory elements, nor did they impact upon the global chromatin topology of the locus. This confirms the observation that even the significant divergence in CREs located at the *HoxD* locus, which accompanied the evolution of the snake body plan, did not result in any substantial alteration of the overall corn-snake *Hoxd* gene interaction map (Guerreiro et al., 2016). Altogether, these observations suggest that internal organization of the TADs at the *HoxD* locus and the specific interaction profiles for various subsets of *Hoxd* target genes are resilient to considerable variation in their CREs.

These results also highlight the somewhat dual properties that large regulatory landscapes may have imposed in the course of regulatory evolution. On the one hand, a pre-established chromatin topology, as materialized by TADs, may have provided unique 'structural niches' to evolve new enhancer sequences, due to the proximity of factors already at work. This might especially apply to landscapes where a strong quantitative parameter may be instrumental, and *a fortiori* when the target gene(s) are acting in combination, coding for proteins of rather low specificities (Bolt and Duboule, 2020). This may be illustrated nowadays by large landscapes, where all kinds of enhancer sequences are mixed within the same TAD. On the other hand, this regulatory playground, while stimulating the emergence of regulations, will constrain their realms of action due both to the very architecture that favours their evolution and to the accessibility to 'a' subset of contiguous target genes as a result of the global distribution of interactions at this precise place of the landscape.

MATERIAL AND METHODS

Mouse strains and chicken eggs

All mutant strains are listed in Table S1 and were backcrossed continuously to Bl6/CBA mixed animals and maintained as heterozygous stocks. Chick embryos from a White Leghorn strain were incubated at 37.5°C and staged according to Hamburger and Hamilton (1951). For genomics analyses, we used the mouse assembly mm10 and the chicken galGal6.

Enhancer cloning and transgenics

The different CRE candidate sequences were amplified using PCR-specific primers (see Table S2) and the Expand High Fidelity PCR system (Roche). Amplified fragments were gel-purified and cloned into the pSK-LacZ vector as in (Beccari et al., 2016). For the transgenesis assays, each LacZ reporter construct was digested

with NotI and KpnI and the restriction fragment encoding the potential enhancer sequence, the beta-globin minimal promoter and the LacZ reporter gene was gel-purified and injected into the male pronucleus of fertilized oocytes. F0 embryos were dissected either at E10, or at E12, fixed and stained for LacZ activity according to standard protocols.

In situ hybridization

The probes used in this study for *in situ* hybridization were either previously reported, or produced by PCR amplification of a fragment subsequently ligated in pGEMT Easy vector (Promega). Primers used to amplify the fragment of interest are listed in Table S2. Digoxigenin (Dig) labeled probes were synthesized *in vitro* by linearizing the respective plasmids using specific restriction enzymes and transcribed *in vitro* either with T7/T3, or Sp6 RNA polymerase (Table S3) and the Dig-RNA labeling mix (Roche). The probes were purified using the RNA easy mini kit. WISH experiments were performed as described in (Woltering et al., 2009). Probes are listed in (Table S3). *In situ* experiments in sections were performed according to (Sockanathan and Sockanathan, 2015). Cryostat sections were prepared after fixing embryos in 4% PFA solution at 4ºC overnight. Subsequently, embryos were washed three times with PBS and passed to increasing sucrose solutions at 4ºC in agitation (15% sucrose solution for 3-4 hours, followed by incubation in 30% sucrose solution overnight)and finally included in OCT blocks. Sections of 20um were obtained with a Leica cryostat and stored at -80ºC.

ChIP-seq

ChIP-seq experiments were performed using the ChIP-IT High sensitivity kit (active motif according to manufacturer instructions with minor modifications). For the mouse samples, 12 pairs of E12 VPss, or one hundred E8.75. PT regions were used, the latter dissected at the level of the 2nd to 4th pair of somites. For the chicken samples, the dorsal skin of five HH35 embryos or the PT or ca. 80 HH19-21 PT regions were isolated. In all cases, the samples were fixed for 10 min in 1% formaldehyde at RT and the crosslinking reaction was quenched with Glycine. Subsequently, nuclei were extracted and sonicated in (Tris HCl pH 8.0 50mM, EDTA 10mM, 1% SDS) to an average fragment size of 200-500bp using a Diagenonode Bioruptor Sonicator. Ca. 10 to 20 µg of sonicated chromatin were diluted tenfold with Dilution buffer (HEPES pH 7.3 20mM, EDTA 1mM, NaCl 150mM, NP40 0.1%) and incubated with 2 µg of anti-H3K27ac antibody (Abcam, ab4729). All buffers contained 1X Complete Proteinase Inhibitor cocktail (EDTA-free; Roche) and 10mM Sodium Butyrate to prevent protein degradation and Histone de-acetylation. Chromatin–antibody complexes were immunoprecipitated with Protein G-coupled agarose beads-purified and de-crosslinked according to manufacturer instructions. Approx 5 to 10 ng of purified DNA were used for ChIP library preparation by the Geneva IGE3 Genomics Platform (University of Geneva) and sequenced to obtain 100-bp single-end reads on an Illumina HiSeq2500 or HiSeq4000 system. ChIP-seq reads processing was done as in (Amândio et al., 2020), using the laboratory Galaxy server (Afgan et al., 2016). Adapters and bad-quality bases were removed with Cutadapt version 1.16 (Martin, 2011) (options -m 15 -q 30 -a GATCGGAAGAGCACACGTCTGAACTCCAGTCAC). Reads were mapped to the mouse genome (mm10) and to the chicken genome (galGla6) using Bowtie2 (v2.3.4.1) (Langmead and Salzberg, 2012)

with standard settings. The coverage was obtained as the output of MACS2 (v2.1.1.20160309) (Zhang et al., 2008) Peak calling was done using MACS2 (v2.1.0.20160309). CTCF motif orientation was assessed using the CTCFBSDB 2.0 database (Ziebarth et al., 2012) with EMBL_M1 identified motifs. H3K27ac ChIP-seq were normalized with the MAnorm model (Shao et al., 2012) using peaks called with MACS2 and a fixed extension of 200 bp. MARs were annotated within the mouse T-DOM (chr2:74,872,605-75,696,338) and the chicken T-DOM (chr7:15856252-16252401). CNEs were used to define corresponding regions in each species. The brain coverage was subtracted from each input file. Each possible genomic window totalizing 30 % (VP) or 50% (PT) of the total T-DOM H3K27ac coverage was computed and the smallest and densest window was annotated as 'MAR'.

4C-seq experiments

4C-seq experiments were performed according to (Noordermeer et al., 2011). Briefly, the tissues were dissected, dissociated with collagenase (Sigma Aldrich/Fluka) and filtered through a 35 micron mesh. Cells were fixed with 2% formaldehyde (in PBS/10%FBS) for 10 min at RT and the reaction was quenched on ice with Glycine. Nuclei were extracted using a cell lysis buffer (Tris pH 7.5 10 mM, NaCl 10 mM, $MgCl_2$ 5 mM, EDTA 0.1 mM,) and stored at -80°C. Approximately 20 pairs of mouse E12 VPs, or 200 E9.5 PT regions dissected at the level of the 2nd to 4th pair of somites, as well as 120 chicken HH19-21 PT samples, were used. Nuclei were digested with NlaIII (New England Biolabs) and ligated with T4 DNA ligase HC (Promega) in diluted conditions to promote intramolecular ligation. Samples were digested again with DpnII (New England Biolabs) and re-ligated with T4 DNA ligase HC. These templates were amplified using Expand long template (Roche) and PCR barcoded primers flanked with adaptors. For each library, 8 to 10 independent PCR reactions were pooled together and purified using the PCR purification kit (Qiagen). Multiplexed libraries were sequenced on Illumina HiSeq 2500 to obtain 100 bp single-end reads. Demultiplexing, mapping and 4C-seq analysis were performed using a local version of the pipeline described in (David et al., 2014), on the mouse GRCm38 (mm10) and chicken GalGal6 genome assemblies. The profiles were smoothened using a window size of 11 fragments and normalized to the mean score in +/-5 Mb around the viewpoint. When multiple independent biological replicates were available, average 4C-seq profiles were calculated.

Capture HiC-seq experiments

Libraries of sureSelect enrichment probes were designed as described in (Bolt et al., 2021) for mouse and (Yakushiji-Kaminatsui et al., 2018) for chicken. Dissected tissues were processed as in (Yakushiji-Kaminatsui et al., 2018) with the following changes: cells were cross-linked in 2% formaldehyde/PBS and washed three times instead of being quenched by glycine. HiC-libraries were prepared as in (Yakushiji-Kaminatsui et al., 2018).

ETHICS APPROVAL

All experiments involving animals were performed in agreement with the Swiss Law on Animal Protection (LPA), under license No GE 81/14 (to DD).

DATA AVAILABILITY

All raw and processed datasets are available in the Gene Expression Omnibus (GEO) repository under accession number GEOXXXXXX

COMPETING INTERESTS

The authors declare that they have no competing interests.

FUNDING

This work was supported by funds from the University of Geneva, the Ecole Polytechnique Fédérale (EPFL, Lausanne), the Swiss National Research Fund (No. 310030B_138662) and the European Research Council grants System*Hox* (No 232790) and Regul*Hox* (No 588029) (to D.D.). Funding bodies had no role in the design of the study and collection, analysis and interpretation of data and in writing the manuscript.

AUTHORS CONTRIBUTIONS

A.I. : Designed experiments, realized experiments and interpreted the results, wrote the manuscript

I.G. : Did some cloning and *in situ* hybridizations

C.C.B. : Provided unpublished datasets and helped for some the C-HiC experiments

S.G. : Genotyped and helped analyze mouse mutants.

D.D. : Designed experiments, interpreted some results and wrote the paper.

L.B. : Designed experiments, interpreted some results and wrote the paper.

ACKNOWLEDGEMENTS

We thank Dr Lucille Lopez-Delisle for her help with bioinformatics as well as members of the Duboule laboratories for comments and discussions and Gregory Loichot for artwork. This work was supported in part by using the resources and services of both the Gene Expression Core Facility at the School of Life Sciences of the EPFL in Lausanne and the genomic plateform from the IGE3 centre of the University of Geneva. Transgene injections were performed at the transgenesis platform of the University of Geneva Medical School. This work was supported by funds from the University of Geneva, the Ecole Polytechnique Fédérale (EPFL, Lausanne), the Swiss National Research Fund (No. 310030B_138662) and the European Research Council

grants SystemHox (No 232790) and RegulHox (No 588029) (to D.D.). Funding bodies had no role in the design of the study and collection, analysis and interpretation of data and in writing the manuscript.

LEGENDS TO FIGURES

Figure 1. Transcription of *Hoxd* genes in mammalian and avian skin primordia. A. Schematic illustration of a E12.5 mouse embryo with VPs (Vibrissae Primordia) represented as red circles. The dorso-ventral (D, V) and the caudo-rostral (C, R) axes are shown as red arrows representing the timing of appearance of the vibrissae primordia. **B.** WISH on E12.5 faces. The arrowheads point to the most caudo-dorsal placode, which is the largest one and the first to appear. Staining intensity progressively decreases from *Hoxd1* to *Hoxd8.* **C.** Schematic illustration of the back of a HH35 chicken embryo with feather placodes as red circles. A, anterior; P, posterior. **D.** WISH on HH35 chicken showing the skin of the upper back. The arrowheads point to the neck at the level of the shoulders. *HOXD1* is not expressed, whereas *HOXD3* and *HOXD8* signal intensities are stronger than for *HOXD4* and *HOXD9.* **E.** Schematic representation of a E9.5 or HH20 posterior trunk and tailbud. A, anterior; P, posterior; PSM, presomitic mesoderm; NT, neural tube; IM, intermediate mesoderm; FS, forming somites; PM, paraxial mesoderm; LM, lateral mesoderm; S, somites. **F.** WISH on E9.5 mouse posterior trunk and tail bud. *Hoxd1* transcription pattern is different from that of *Hoxd3* and *Hoxd4.* **G.** WISH on HH20 chicken posterior trunk and tail bud. *HOXD1* transcription pattern is different from *HOXD3* and *HOXD4.* The white arrowheads in panels **F** and **G** point to the *Hoxd1* stripe in the PSM. The black arrowheads show the difference between mouse (**F**) and chicken (**G**) in the *Hoxd1* mRNAs persistence in formed somites.

Figure 2. Capture HiC-seq at the mouse and chicken *HoxD* loci. A, **B.** Capture HiC-seq heatmaps using dissected posterior trunk cells. Below each heatmap, a CTCF ChIP-seq track is shown, produced from the same material. The similarities in the structural organization of the mouse and the chicken loci are underlined either by the positions of syntenic CNEs at key positions (numbered vertical dashed lines), the domains produced by TAD calling (black bars below) and the presence of a sub-TAD boundary (asterisk) within T-DOM. Genes are represented by empty rectangles. In panel **A,** E9.5 mouse PT cells were used and the CHiC heatmap was mapped on mm10 with a bin size of 5 kb (chr2:73800000-75800000). In panel **B,** HH20 chicken PT cells were used and the CHiC heatmap mapped on galGal6 with a bin size of 2.5kb (chr7:15790000-16700000). The positions of the two TADs (T-DOM and C-DOM) and of both sub-TADs are shown on top. The scales on the X axes were adjusted to comparable sizes for ease of comparison, yet the chicken locus is more compacted (see the scale bars, bottom right).

Figure 3. Tissue- and gene-specific interactions of dense H3K27ac regions. A. On top is a ChIP-seq profile of H3K27ac using mouse E12.5 VPs (orange) superimposed over the E12.5 forebrain cells (grey) (mm10, chr2:73800000-75800000). Below is a H3K27ac profile produced from dissected chicken HH35 dorsal skin (green), with HH18 brain cells (grey)(galGal6, chr7:15790000-16700000. The highest interacting regions are depicted as D1, D4 and D9 (see Figure S3B). The positions of conserved CNEs were used to delimit these regions in both species (vertical dashed lines) and the extents of TADs are shown below (thick black lines).

The region in T-DOM containing 30 percent of the total T-DOM acetylation (Most Acetylated Region; MAR) is shown as a red rectangle. In the mouse VP, the MAR is within the D1 DNA segment, whereas the chicken MAR overlaps with the D4 and D9 regions. **B.** H3K27ac ChIP-seq using mouse E9.5 posterior trunk cells (orange) superimposed over forebrain cells (grey)(mm10, chr2:73800000-75800000. Below is shown the H3K27ac profile obtained from the same sample but dissected from a HH18 chicken embryo (green) with brain cells (grey) as a control (galGal6, chr7:15790000-16700000). While the mouse PT Most Acetylated Region (MAR, red rectangle) coincides with the D4 segment, the chicken MAR counterpart also covers D4 and a small part of D9.

Figure 4. Regulation of *Hoxd1*. A. WISH using a *Hoxd1* probe on E12.5 mouse embryos. **B**. X-gal staining on E12.5 mouse embryos carrying randomly integrated BACs. **C**. The three deletion lines used are shown (red) as well as the transgenic BACs (blue). The extent of the D1 to D9 regions are shown on top (black) as well as the positions of both sub-TADs below (thick black lines). *Hoxd1* mRNAs were detected in both the control and the Del(SB2-SB3) lines (**A**, (red arrowheads), yet the signal was absent from Del(Attp-SB2) mutant embryos (**A**, white arrowheads). For transgenics, a strong staining was detected in VPs when BAC^{Mtx2} was used (**B**, red arrowhead), whereas staining was not scored with the other two flanking BAC clones (**B**, white arrowheads). Therefore, a region directly downstream the *HoxD* cluster is necessary and sufficient to activate *Hoxd1* transcription in VPs, referred to as Vibrissa Primordium Regulatory Region (**C**, VPRR). **D.** Enlargement of the VPRR region along with a H3K27ac ChIP-seq using dissected E12.5 VPs (orange) superimposed over E12.5 forebrain (FB) cells (grey)(mm10; chr2:74765140-74913171). Above the profiles are the four VPAEs (open arrowheads) and below are MACS2 narrowPeaks for VPs (orange) and FB (grey). The position of the four sequences containing VPAEs and used as transgenes (tgVPAEs) are shown by numbered black boxes (bottom, Figure S5C). **E.** X-gal staining in VPs on a E12.5 embryo transgenic for VPAE2. **F.** WISH of *Hoxd1* on E9.5 embryos focusing on tail buds. *Hoxd1* was detected in forming somites (FS) in both the control and the Del(SB2-SB3) lines (red arrowheads), but was absent from Del(Attp-SB2) mutant embryos (white arrowhead). **G.** X-gal staining of E9.5 mouse embryos carrying various BAC transgenes. Staining was scored in the entire neural tube and paraxial mesoderm with the BAC^{HoxD} (black arrowhead). In contrast, embryos carrying BAC^{Mtx2} displayed staining in forming somites (red arrowhead), a staining absent when BAC^{T1} was used (white arrowhead). **H.** H3K27ac ChIP-seq over the VPRR region using E9.5 PT cells (orange) superimposed over E12.5 FB cells (grey). Above the profiles are the two SAE sequences (black arrowheads) and below are MACS2 narrowPeaks for PT (orange) and FB (grey) cells. The position of the SAE sequence used as a transgene is shown as a red box (tgSAE). **I.** X-gal staining in forming somites on E9.5 embryo transgenic for the VPAE3 sequence.

Figure 5. Conserved sequences with divergent functions. A. Bar plots showing the proportion of putative *cis*-regulatory elements (pCREs) harboring the H3K27ac mark in one ('specific') *versus* more than one ('pleiotropic') tissues, in either mouse (orange) or chicken (green). For simplification purposes, distal pCREs (>2kb away from the transcription start site) are referred as 'enhancers' and proximal pCREs (<2kb away from

transcription start site) are called 'promoters'. The different proportions are shwon when comparing enhancers and promoters (left), and conserved enhancers to non-conserved enhancers (right). The proportion of specific *versus* pleiotropic elements is shown for conserved and non-conserved enhancers (right). In both mouse and chicken, enhancers are more specific than promoters and amongst enhancers, conserved elements are found acetylated in more tissues than non-conserved elements. **B.** Heatmap obtained using pheatmap R package. On the *X*-axis are shown enhancer-CNEs i.e., conserved sequences, which are non-coding in mouse and in chicken and which overlap with a H3K27ac mark in at least one species. On the *Y*-axis are displayed those tissues used to obtain MACS2 processed peaks. Tissue-specific activity (H3K27ac-positive) is shown in red, whereas abence of H3K27ac is in blue. FB, forebrain; PFL, proximal forelimb; DFL, distal forelimb; PT, posterior trunk; DS, dorsal skin. CNEs cluster exactly by species. **C.** Euler plots representing the proportion of enhancer-CNEs, per tissue, acetylated in mouse only (orange), chicken only (green), or both (pistachio). In **B** and **C,** FB, forebrain; PL, proximal limb; DL, distal limb; PT, posterior trunk; DS, dorsal skin.

LEGENDS TO SUPPLEMENTARY FIGURES

Supplementary Figure S1. Evolution of the *HoxD* locus and expression of *Hoxd* genes in the developing VPs. A. On the left is a schematic illustration of a vertebrate phylogenetic tree showing the emergence of some skin derivatives (glands, scales, feathers, hairs). On the right are the corresponding versions of the *HoxD* locus, with the orthologous *HoxD* gene clusters as shaded orange areas and other orthologous genes shown in green to help delimit the extent of the conserved regulatory landscapes. **B.** Schematic of the transversal section on E13.5 VPs (left), analyzed in ISH with a *Hoxd1* probe (right). The scale bar in the right picture corresponds to 100 µm and the *Hoxd1* stained VPs at peg stage (see below) are indicated by red arrowheads of decreasing intensities. The staining is localized in dermal cells. **C.** WISH on E12.5 bisected mouse embryos. *Hoxd1* mRNAs were detected after those for *Shh* (left) and before *Hoxd4* mRNAs (right). **D.** Schematic representation of vibrissae morphogenesis: epithelial placode (EP, yellow cells); dermal condensation (DC, blue cells). The approximate developmental stage is indicated below, showing the delay between vibrissae and hair morphogenesis. The dorsal skin of the upper back was used as reference for hairs. **E.** WISH on three successive E12 staged embryos (indicated on the left) using four *Hoxd* genes as probes (top). The same three placodes are pointed by red (positive) or white (negative).

Supplementary Figure S2. Feather development and transcription of *Hoxd* genes. A. Schematic of feather development between stage HH20 and HH35 with ectodermal placode (EP, yellow) and dermal condensation cells (DC, blue). **B**. Transversal plan through a HH35 chicken skin of the upper back (red), corresponding to the two sections stained by ISH on the right. The scale bar is 100 µm. *SHH* is used as marker of the epithelial placode (red arrowhead) and *HOXD8* is transcribed in epithelial placodes, matching -or slightly larger than- the *SHH* domain. **C.** WISH on HH35 chicken embryos, dorsal view of the upper back, with arrowheads pointing toward the neck at the shoulder level. *HOXD11* transcripts were not detected in FPs, unlike those of SHH.

Supplementary Figure S3. Comparative 4C-seq analyses at the mouse and chicken *HoxD* loci. A. Synteny plots representing sequences conserved between the mouse and the chicken *HoxD* loci. On the X-axis is the mouse locus (mm10, chr2:73800000-75800000) and on the Y axis is the chicken locus (galGal6, chr7:15790000-16700000). The scale is the same for both axes. TADs and sub-TADs are indicated by black lines and the *HoxD* cluster by a red rectangle. Schematic representations of the locus are on top of each axis. Despite a mouse locus that is in average 2.2 times larger than its chicken counterpart, the order of the conserved sequences is maintained, showing the absence of substantial genomic rearrangement at this locus. **B**. On the Y axis are 4C-seq normalised scores per feature, with E9.5 mouse PT cells scores (orange) superimposed over E12.5 FB cells (grey). Below the 4C tracks, the positions of the *Hoxd1, Hoxd4* and *Hoxd9* viewpoints are represented by triangles, with a black triangle for the viewpoint used in the track. Between each track, the subtraction of the two adjacent viewpoints is represented (black). The preferentially interacting regions D1, D4 and D9 were annotated manually and, to facilitate comparisons between their positions in the mouse and the chicken locus, orthologous CNEs located at the edge of each region D are shown (vertical dashed lines). CTCF ChIP-seq profiles are displayed below the 4C tracks, with red and blue arrowheads below indicating their orientation. Color intensity is proportional to motif score. Data mapped on mm10, chr2:73800000-75800000. **C.** On the Y axis are 4C-seq normalised scores per feature, using HH18 chicken PT cells (green), superimposed with the profile obtained with HH18 brain cells (grey). Data shown for *HOXD1* (top) *HOXD4* (middle) and *HOXD9* (bottom) viewpoints, with a black arrowhead indicating the position of the viewpoint. Reads mapped on galGal6, chr7:15790000-16700000.

Supplementary Figure S4. Comparison of conserved and non-conserved CREs in mouse and chicken embryonic tissues. A. H3K27ac ChIP-seq profiles enlarged over the mouse and chicken VPRR (mm10, chr2:74775737-75222876). Top: Mouse E12.5 dissected VPs (orange) along with the mouse E12.5 forebrain cells track (grey). Below is the profile for the chicken HH35 dorsal skin (green), superimposed to HH18 brain cells (grey) (GalGal6, chr7:16033612-16252401). Processed MACS2 narrowPeaks are in orange/green vertical lines and BLAST (reference) conserved sequences in black vertical lines, below each track. The peaks overlapping CNEs are pointed by black arrows. The peaks corresponding to CNEs in both species and in equivalent tissues are pointed by red arrows. Vertical dashed lines represent the position of corresponding CNEs at the edge of each region **B.** H3K27ac ChIP-seq focusing on VPRR. Top: The profile for mouse E9.5 posterior trunk cells (orange) are superimposed to mouse E12.5 forebrain cells (grey). Bottom: Profiles of chicken HH18 embryonic posterior trunk cells (green) and of HH18 brain cells.

Supplementary Figure S5. *Hoxd1* regulation in mouse vibrissae primordia (VP) and posterior trunk (PT) cells. A. Along the Y-axis are 4C-seq normalised score per feature using E12.5 dissected mouse VPs (orange), superimposed (braun) over E12.5 brain cells as control (grey). Below the 4C tracks, the positions of the *Hoxd1, Hoxd4* and *Hoxd9* viewpoints are represented by triangles with the viewpoint used in the track in black. Between each track is the subtraction of PT to VPs scores (dark braun). The data are mapped on

mm10 (chr2:73800000-75800000). The positions of the D1, D4 and D9 regions are shown on top and the TADs are indicated with thick black lines at the bottom. The vertical dashed lines correspond to orthologous CNEs used for positioning the various regions **B.** VISTA alignments of sequences used as transgenes, to visualize nucleotide conservation. Species are on the left, sequences on top. **C.** X-gal staining of E12.5 embryos carrying transgenes that are not reporting any regulatory activity in VPs (tg^{VPAE1}, tg^{VPAE3}, tg^{VPAE4}) **D.** S-gal staining of a E9.5 mouse embryo transgenic for the tg^{SAE} sequence, showing no staining in forming somites.

Supplementary Figure S6. Lineage-specific H3K27ac-positive elements active in chicken FPAEs. A. ChIP H3K27ac profile using either dissected chicken HH35 dorsal skin (green), or HH18 brain cells (grey) over the MAR region defined in Figure 3. **B.** VISTA alignments of sequences specifically enriched for the H327ac epigenetic mark in the embryonic chicken skin (HH35), but not in the brain and posterior trunk samples, and located within the FPAR. Species are on the left, sequences on top. No significant homology of these elements was found within the mouse *HoxD* genomic region.

LEGENDS TO SUPPLEMENTARY TABLES

Supplementary Table S1. List of mouse lines

Supplementary Table S2. Primers used to clone candidate enhancer sequences

Supplementary Table S3. Probes for *in situ* hybridization

BIBLIOGRAPHY

Acemel, R.D., Tena, J.J., Irastorza-Azcarate, I., Marlétaz, F., Gómez-Marín, C., de la Calle-Mustienes, E., Bertrand, S., Diaz, S.G., Aldea, D., Aury, J.-M., Mangenot, S., Holland, P.W.H., Devos, D.P., Maeso, I., Escrivá, H., Gómez-Skarmeta, J.L., 2016. A single three-dimensional chromatin compartment in amphioxus indicates a stepwise evolution of vertebrate Hox bimodal regulation. Nat. Genet. 48, 336–341. https://doi.org/10.1038/ng.3497

Afgan, E., Baker, D., van den Beek, M., Blankenberg, D., Bouvier, D., Čech, M., Chilton, J., Clements, D., Coraor, N., Eberhard, C., Grüning, B., Guerler, A., Hillman-Jackson, J., Von Kuster, G., Rasche, E., Soranzo, N., Turaga, N., Taylor, J., Nekrutenko, A., Goecks, J., 2016. The Galaxy platform for accessible, reproducible and collaborative biomedical analyses: 2016 update. Nucleic Acids Res. 44, W3–W10. https://doi.org/10.1093/nar/gkw343

Allais-Bonnet, A., Hintermann, A., Deloche, M.-C., Cornette, R., Bardou, P., Naval-Sanchez, M., Pinton, A., Haruda, A., Grohs, C., Zakany, J., Bigi, D., Medugorac, I., Putelat, O., Greyvenstein, O., Hadfield, T., Jemaa, S.B., Bunevski, G., Menzi, F., Hirter, N., Paris, J.M., Hedges, J., Palhiere, I., Rupp, R., Lenstra, J.A., Gidney, L., Lesur, J., Schafberg, R., Stache, M., Wandhammer, M.-D., Arbogast, R.-M., Guintard, C., Blin, A., Boukadiri, A., Rivière, J., Esquerré, D., Donnadieu, C., Danchin-Burge, C., Reich, C.M., Riley, D.G., Marle-Koster, E. van, Cockett, N., Hayes, B.J., Drögemüller, C., Kijas, J., Pailhoux, E., Tosser-Klopp, G., Duboule, D., Capitan, A., 2021. Analysis of Polycerate Mutants Reveals the Evolutionary Co-option of *HOXD1* for Horn Patterning in Bovidae. Mol. Biol. Evol. 38, 2260–2272. https://doi.org/10.1093/molbev/msab021

Amândio, A.R., Lopez-Delisle, L., Bolt, C.C., Mascrez, B., Duboule, D., 2020. A complex regulatory landscape involved in the development of mammalian external genitals. eLife 9, e52962. https://doi.org/10.7554/eLife.52962

Ambrosino, L., Vassalli, Q.A., D'Agostino, Y., Esposito, R., Cetrangolo, V., Caputi, L., Amoroso, A., Aniello, F., D'Aniello, S., Chatzigeorgiou, M., Chiusano, M.L., Locascio, A., 2019. Functional conserved non-coding elements among tunicates and chordates. Dev. Biol., Current Directions in Tunicate Development 448, 101–110. https://doi.org/10.1016/j.ydbio.2018.12.012

Andrey, G., Montavon, T., Mascrez, B., Gonzalez, F., Noordermeer, D., Leleu, M., Trono, D., Spitz, F., Duboule, D., 2013. A switch between topological domains underlies HoxD genes collinearity in mouse limbs. Science 340, 1234167. https://doi.org/10.1126/science.1234167

Beccari, L., Yakushiji-Kaminatsui, N., Woltering, J.M., Necsulea, A., Lonfat, N., Rodriguez-Carballo, E., Mascrez, B., Yamamoto, S., Kuroiwa, A., Duboule, D., 2016. A role for HOX13 proteins in the regulatory switch between TADs at the HoxD locus. Genes Dev. 30, 1172–1186. https://doi.org/10.1101/gad.281055.116

Belton, J.-M., McCord, R.P., Gibcus, J., Naumova, N., Zhan, Y., Dekker, J., 2012. Hi-C: A comprehensive technique to capture the conformation of genomes. Methods San Diego Calif 58. https://doi.org/10.1016/j.ymeth.2012.05.001

Berthelot, C., Villar, D., Horvath, J.E., Odom, D.T., Flicek, P., 2018. Complexity and conservation of regulatory landscapes underlie evolutionary resilience of mammalian gene expression. Nat. Ecol. Evol. 2, 152–163. https://doi.org/10.1038/s41559-017-0377-2

Biggs, L.C., Mikkola, M.L., 2014. Early inductive events in ectodermal appendage morphogenesis.

Bolt, C.C., Duboule, D., 2020. The regulatory landscapes of developmental genes. Development 147, dev171736. https://doi.org/10.1242/dev.171736

Bolt, C.C., Lopez-Delisle, L., Mascrez, B., Duboule, D., 2021. MESOMELIC DYSPLASIAS ASSOCIATED WITH THE HOXD LOCUS ARE CAUSED BY REGULATORY REALLOCATIONS. bioRxiv 2021.02.01.429171. https://doi.org/10.1101/2021.02.01.429171

Carroll, S.B., 2008. Evo-Devo and an Expanding Evolutionary Synthesis: A Genetic Theory of Morphological Evolution. Cell 134, 25–36. https://doi.org/10.1016/j.cell.2008.06.030

Chiang, C., Swan, R.Z., Grachtchouk, M., Bolinger, M., Litingtung, Y., Robertson, E.K., Cooper, M.K., Gaffield, W., Westphal, H., Beachy, P.A., Dlugosz, A.A., 1999. Essential role for Sonic

hedgehog during hair follicle morphogenesis. Dev. Biol. 205, 1–9. https://doi.org/10.1006/dbio.1998.9103
Chuong, C.M., Oliver, G., Ting, S.A., Jegalian, B.G., Chen, H.M., De Robertis, E.M., 1990. Gradients of homeoproteins in developing feather buds. Dev. Camb. Engl. 110, 1021–1030.
Creyghton, M.P., Cheng, A.W., Welstead, G.G., Kooistra, T., Carey, B.W., Steine, E.J., Hanna, J., Lodato, M.A., Frampton, G.M., Sharp, P.A., Boyer, L.A., Young, R.A., Jaenisch, R., 2010. Histone H3K27ac separates active from poised enhancers and predicts developmental state. Proc Natl Acad Sci USA 107, 21931–21936. https://doi.org/10.1073/pnas.1016071107
Dale, K.J., Pourquié, O., 2000. A clock-work somite. BioEssays 22, 72–83. https://doi.org/10.1002/(SICI)1521-1878(200001)22:1<72::AID-BIES12>3.0.CO;2-S
Darbellay, F., Bochaton, C., Lopez-Delisle, L., Mascrez, B., Tschopp, P., Delpretti, S., Zakany, J., Duboule, D., 2019. The constrained architecture of mammalian Hox gene clusters. Proc. Natl. Acad. Sci. U. S. A. 116, 13424–13433. https://doi.org/10.1073/pnas.1904602116
Darbellay, F., Duboule, D., 2016. Chapter Sixteen - Topological Domains, Metagenes, and the Emergence of Pleiotropic Regulations at Hox Loci, in: Wassarman, P.M. (Ed.), Current Topics in Developmental Biology, Essays on Developmental Biology, Part A. Academic Press, pp. 299–314.
David, F.P.A., Delafontaine, J., Carat, S., Ross, F.J., Lefebvre, G., Jarosz, Y., Sinclair, L., Noordermeer, D., Rougemont, J., Leleu, M., 2014. HTSstation: A Web Application and Open-Access Libraries for High-Throughput Sequencing Data Analysis. PLoS ONE 9, e85879. https://doi.org/10.1371/journal.pone.0085879
Dekker, J., Heard, E., 2015. Structural and functional diversity of Topologically Associating Domains. FEBS Lett. 589, 2877–2884. https://doi.org/10.1016/j.febslet.2015.08.044
Delpretti, S., Montavon, T., Leleu, M., Joye, E., Tzika, A., Milinkovitch, M., Duboule, D., 2013. Multiple enhancers regulate Hoxd genes and the Hotdog LncRNA during cecum budding. Cell Rep. 5, 137–50. https://doi.org/10.1016/j.celrep.2013.09.002
Dermitzakis, E.T., Clark, A.G., 2002. Evolution of Transcription Factor Binding Sites in Mammalian Gene Regulatory Regions: Conservation and Turnover. Mol. Biol. Evol. 19, 1114–1121. https://doi.org/10.1093/oxfordjournals.molbev.a004169
Dhouailly, D., 2009. A new scenario for the evolutionary origin of hair, feather, and avian scales. J. Anat. 214, 587–606. https://doi.org/10.1111/j.1469-7580.2008.01041.x
Dhouailly, D., Godefroit, P., Martin, T., Nonchev, S., Caraguel, F., Oftedal, O., 2019. Getting to the root of scales, feather and hair: As deep as odontodes? Exp. Dermatol. 28, 503–508. https://doi.org/10.1111/exd.13391
Di-Poï, N., Milinkovitch, M.C., 2016. The anatomical placode in reptile scale morphogenesis indicates shared ancestry among skin appendages in amniotes. Sci. Adv. 2, e1600708. https://doi.org/10.1126/sciadv.1600708
Dixon, J.R., Gorkin, D.U., Ren, B., 2016. Chromatin Domains: The Unit of Chromosome Organization. Mol. Cell 62, 668–680. https://doi.org/10.1016/j.molcel.2016.05.018
Dixon, J.R., Selvaraj, S., Yue, F., Kim, A., Li, Y., Shen, Y., Hu, M., Liu, J.S., Ren, B., 2012. Topological Domains in Mammalian Genomes Identified by Analysis of Chromatin Interactions. Nature 485, 376–380. https://doi.org/10.1038/nature11082
Edwards, S.L., Beesley, J., French, J.D., Dunning, A.M., 2013. Beyond GWASs: Illuminating the Dark Road from Association to Function. Am. J. Hum. Genet. 93, 779–797. https://doi.org/10.1016/j.ajhg.2013.10.012
Eichenlaub, M.P., Ettwiller, L., 2011. De Novo Genesis of Enhancers in Vertebrates. PLoS Biol. 9. https://doi.org/10.1371/journal.pbio.1001188
Eres, I.E., Luo, K., Hsiao, C.J., Blake, L.E., Gilad, Y., 2019. Reorganization of 3D genome structure may contribute to gene regulatory evolution in primates. PLOS Genet. 15, e1008278. https://doi.org/10.1371/journal.pgen.1008278
Fernandez-Guerrero, M., Yakushiji-Kaminatsui, N., Lopez-Delisle, L., Zdral, S., Darbellay, F., Perez-Gomez, R., Bolt, C.C., Sanchez-Martin, M.A., Duboule, D., Ros, M.A., 2020. Mammalian-

specific ectodermal enhancers control the expression of Hoxc genes in developing nails and hair follicles. Proc. Natl. Acad. Sci. U. S. A. 117, 30509–30519. https://doi.org/10.1073/pnas.2011078117
Gaunt, S.J., 1988. Mouse homeobox gene transcripts occupy different but overlapping domains in embryonic germ layers and organs: a comparison of Hox-3.1 and Hox-1.5. Development 103, 135–44.
Godwin, A.R., Capecchi, M.R., 1998. Hoxc13 mutant mice lack external hair. Genes Dev. 12, 11–20.
Guerreiro, I., Gitto, S., Novoa, A., Codourey, J., Nguyen Huynh, T.H., Gonzalez, F., Milinkovitch, M.C., Mallo, M., Duboule, D., 2016. Reorganisation of Hoxd regulatory landscapes during the evolution of a snake-like body plan. eLife 5, e16087. https://doi.org/10.7554/eLife.16087
Hamburger, V., Hamilton, H.L., 1951. A series of normal stages in the development of the chick embryo. J. Morphol. 88, 49–92. https://doi.org/10.1002/jmor.1050880104
Hansen, A.S., Pustova, I., Cattoglio, C., Tjian, R., Darzacq, X., 2017. CTCF and cohesin regulate chromatin loop stability with distinct dynamics. eLife 6, e25776. https://doi.org/10.7554/eLife.25776
Harmston, N., Ing-Simmons, E., Tan, G., Perry, M., Merkenschlager, M., Lenhard, B., 2017. Topologically associating domains are ancient features that coincide with Metazoan clusters of extreme noncoding conservation. Nat. Commun. 8. https://doi.org/10.1038/s41467-017-00524-5
Holland, L.Z., Albalat, R., Azumi, K., Benito-Gutiérrez, È., Blow, M.J., Bronner-Fraser, M., Brunet, F., Butts, T., Candiani, S., Dishaw, L.J., Ferrier, D.E.K., Garcia-Fernàndez, J., Gibson-Brown, J.J., Gissi, C., Godzik, A., Hallböök, F., Hirose, D., Hosomichi, K., Ikuta, T., Inoko, H., Kasahara, M., Kasamatsu, J., Kawashima, T., Kimura, A., Kobayashi, M., Kozmik, Z., Kubokawa, K., Laudet, V., Litman, G.W., McHardy, A.C., Meulemans, D., Nonaka, M., Olinski, R.P., Pancer, Z., Pennacchio, L.A., Pestarino, M., Rast, J.P., Rigoutsos, I., Robinson-Rechavi, M., Roch, G., Saiga, H., Sasakura, Y., Satake, M., Satou, Y., Schubert, M., Sherwood, N., Shiina, T., Takatori, N., Tello, J., Vopalensky, P., Wada, S., Xu, A., Ye, Y., Yoshida, K., Yoshizaki, F., Yu, J.-K., Zhang, Q., Zmasek, C.M., Jong, P.J. de, Osoegawa, K., Putnam, N.H., Rokhsar, D.S., Satoh, N., Holland, P.W.H., 2008. The amphioxus genome illuminates vertebrate origins and cephalochordate biology. Genome Res. 18, 1100–1111. https://doi.org/10.1101/gr.073676.107
Holland, P.W.H., Garcia-Fernàndez, J., 1996. HoxGenes and Chordate Evolution. Dev. Biol. 173, 382–395. https://doi.org/10.1006/dbio.1996.0034
Irimia, M., Tena, J.J., Alexis, M.S., Fernandez-Miñan, A., Maeso, I., Bogdanovic, O., de la Calle-Mustienes, E., Roy, S.W., Gómez-Skarmeta, J.L., Fraser, H.B., 2012. Extensive conservation of ancient microsynteny across metazoans due to cis-regulatory constraints. Genome Res. 22, 2356–2367. https://doi.org/10.1101/gr.139725.112
Kanzler, B., Prin, F., Thelu, J., Dhouailly, D., 1997. CHOXC-8 and CHOXD-13 expression in embryonic chick skin and cutaneous appendage specification. Dev. Dyn. Off. Publ. Am. Assoc. Anat. 210, 274–287. https://doi.org/10.1002/(SICI)1097-0177(199711)210:3<274::AID-AJA8>3.0.CO;2-D
Kanzler, B., Viallet, J.P., Le Mouellic, H., Boncinelli, E., Duboule, D., Dhouailly, D., 1994. Differential expression of two different homeobox gene families during mouse tegument morphogenesis. Int. J. Dev. Biol. 38, 633–640.
Kragesteen, B.K., Spielmann, M., Paliou, C., Heinrich, V., Schöpflin, R., Esposito, A., Annunziatella, C., Bianco, S., Chiariello, A.M., Jerković, I., Harabula, I., Guckelberger, P., Pechstein, M., Wittler, L., Chan, W.-L., Franke, M., Lupiáñez, D.G., Kraft, K., Timmermann, B., Vingron, M., Visel, A., Nicodemi, M., Mundlos, S., Andrey, G., 2018. Dynamic 3D chromatin architecture contributes to enhancer specificity and limb morphogenesis. Nat. Genet. 50, 1463–1473. https://doi.org/10.1038/s41588-018-0221-x
Langmead, B., Salzberg, S.L., 2012. Fast gapped-read alignment with Bowtie 2. Nat Methods 9, 357–9. https://doi.org/10.1038/nmeth.1923

Laverré, A., Tannier, E., Necsulea, A., 2021. Long-range promoter-enhancer contacts are conserved during evolution and contribute to gene expression robustness. bioRxiv 2021.02.26.432473. https://doi.org/10.1101/2021.02.26.432473
Liao, Y., Zhang, X., Chakraborty, M., Emerson, J.J., 2021. Topologically associating domains and their role in the evolution of genome structure and function in Drosophila. Genome Res. 31, 397–410. https://doi.org/10.1101/gr.266130.120
Long, H.K., Prescott, S.L., Wysocka, J., 2016. Ever-Changing Landscapes: Transcriptional Enhancers in Development and Evolution. Cell 167, 1170–1187. https://doi.org/10.1016/j.cell.2016.09.018
Lupiáñez, D.G., Kraft, K., Heinrich, V., Krawitz, P., Brancati, F., Klopocki, E., Horn, D., Kayserili, H., Opitz, J.M., Laxova, R., Santos-Simarro, F., Gilbert-Dussardier, B., Wittler, L., Borschiwer, M., Haas, S.A., Osterwalder, M., Franke, M., Timmermann, B., Hecht, J., Spielmann, M., Visel, A., Mundlos, S., 2015. Disruptions of Topological Chromatin Domains Cause Pathogenic Rewiring of Gene-Enhancer Interactions. Cell 161, 1012–1025. https://doi.org/10.1016/j.cell.2015.04.004
Marinic, M., Aktas, T., Ruf, S., Spitz, F., 2013. An integrated holo-enhancer unit defines tissue and gene specificity of the Fgf8 regulatory landscape. Dev. Cell 24, 530–42. https://doi.org/10.1016/j.devcel.2013.01.025
Martin, M., 2011. Cutadapt removes adapter sequences from high-throughput sequencing reads. EMBnet.journal 17. https://doi.org/10.14806/ej.17.1.200
Michon, F., Charveron, M., Dhouailly, D., 2007. Dermal condensation formation in the chick embryo: Requirement for integrin engagement and subsequent stabilization by a possible Notch/integrin interaction. Dev. Dyn. 236, 755–768. https://doi.org/10.1002/dvdy.21080
Mikkola, M.L., 2007. Genetic basis of skin appendage development. Semin. Cell Dev. Biol., Mechanisms and biological significance of RNA localization AND Development of ectodermal appendages 18, 225–236. https://doi.org/10.1016/j.semcdb.2007.01.007
Montavon, T., Soshnikova, N., Mascrez, B., Joye, E., Thevenet, L., Splinter, E., de Laat, W., Spitz, F., Duboule, D., 2011. A Regulatory Archipelago Controls Hox Genes Transcription in Digits. Cell 147, 1132–1145. https://doi.org/10.1016/j.cell.2011.10.023
Nanni, L., Ceri, S., Logie, C., 2020. Spatial patterns of CTCF sites define the anatomy of TADs and their boundaries. Genome Biol. 21, 197. https://doi.org/10.1186/s13059-020-02108-x
Noordermeer, D., Leleu, M., Splinter, E., Rougemont, J., De Laat, W., Duboule, D., 2011. The dynamic architecture of Hox gene clusters. Science 334, 222–5. https://doi.org/10.1126/science.1207194
Nora, E.P., Lajoie, B.R., Schulz, E.G., Giorgetti, L., Okamoto, I., Servant, N., Piolot, T., Berkum, N.L. van, Meisig, J., Sedat, J., Gribnau, J., Barillot, E., Blüthgen, N., Dekker, J., Heard, E., 2012. Spatial partitioning of the regulatory landscape of the X-inactivation centre. Nature 485, 381. https://doi.org/10.1038/nature11049
Packer, A.I., Jane-wit, D., McLean, L., Panteleyev, A.A., Christiano, A.M., Wolgemuth, D.J., 2000. Hoxa4 expression in developing mouse hair follicles and skin. Mech. Dev. 99, 153–157. https://doi.org/10.1016/S0925-4773(00)00471-8
Pantalacci, S., Chaumot, A., Benoît, G., Sadier, A., Delsuc, F., Douzery, E.J.P., Laudet, V., 2008. Conserved features and evolutionary shifts of the EDA signaling pathway involved in vertebrate skin appendage development. Mol. Biol. Evol. 25, 912–928. https://doi.org/10.1093/molbev/msn038
Pugacheva, E.M., Kubo, N., Loukinov, D., Tajmul, M., Kang, S., Kovalchuk, A.L., Strunnikov, A.V., Zentner, G.E., Ren, B., Lobanenkov, V.V., 2020. CTCF mediates chromatin looping via N-terminal domain-dependent cohesin retention. Proc. Natl. Acad. Sci. U. S. A. 117, 2020–2031. https://doi.org/10.1073/pnas.1911708117
Rada-Iglesias, A., Bajpai, R., Swigut, T., Brugmann, S.A., Flynn, R.A., Wysocka, J., 2011. A unique chromatin signature uncovers early developmental enhancers in humans. Nature 470, 279–283. https://doi.org/10.1038/nature09692

Rao, S.S.P., Huntley, M.H., Durand, N.C., Stamenova, E.K., Bochkov, I.D., Robinson, J.T., Sanborn, A.L., Machol, I., Omer, A.D., Lander, E.S., Aiden, E.L., 2014. A 3D Map of the Human Genome at Kilobase Resolution Reveals Principles of Chromatin Looping. Cell 159, 1665–1680. https://doi.org/10.1016/j.cell.2014.11.021
Rebeiz, M., Patel, N.H., Hinman, V.F., 2015. Unraveling the Tangled Skein: The Evolution of Transcriptional Regulatory Networks in Development. Annu. Rev. Genomics Hum. Genet. 16, 103–131. https://doi.org/10.1146/annurev-genom-091212-153423
Reid, A.I., Gaunt, S.J., 2002. Colinearity and non-colinearity in the expression of Hox genes in developing chick skin. Int. J. Dev. Biol. 46, 209–15. https://doi.org/10.1387/ijdb.011495
Reynolds, A.J., Lawrence, C.M., Jahoda, C.A., 1995. Hair follicle and fiber reconstruction. J. Invest. Dermatol. 104, 39S-40S. https://doi.org/10.1038/jid.1995.57
Rodríguez-Carballo, E., Lopez-Delisle, L., Willemin, A., Beccari, L., Gitto, S., Mascrez, B., Duboule, D., 2020. Chromatin topology and the timing of enhancer function at the HoxD locus. Proc. Natl. Acad. Sci. U. S. A. 117, 31231–31241. https://doi.org/10.1073/pnas.2015083117
Rodriguez-Carballo, E., Lopez-Delisle, L., Zhan, Y., Fabre, P.J., Beccari, L., El-Idrissi, I., Huynh, T.H.N., Ozadam, H., Dekker, J., Duboule, D., 2017. The HoxD cluster is a dynamic and resilient TAD boundary controlling the segregation of antagonistic regulatory landscapes. Genes Dev. 31, 2264–2281. https://doi.org/10.1101/gad.307769.117
Sabari, B.R., Dall'Agnese, A., Boija, A., Klein, I.A., Coffey, E.L., Shrinivas, K., Abraham, B.J., Hannett, N.M., Zamudio, A.V., Manteiga, J.C., Li, C.H., Guo, Y.E., Day, D.S., Schuijers, J., Vasile, E., Malik, S., Hnisz, D., Lee, T.I., Cisse, I.I., Roeder, R.G., Sharp, P.A., Chakraborty, A.K., Young, R.A., 2018. Coactivator condensation at super-enhancers links phase separation and gene control. Science 361. https://doi.org/10.1126/science.aar3958
Sandelin, A., Bailey, P., Bruce, S., Engström, P.G., Klos, J.M., Wasserman, W.W., Ericson, J., Lenhard, B., 2004. Arrays of ultraconserved non-coding regions span the loci of key developmental genes in vertebrate genomes. BMC Genomics 5, 99. https://doi.org/10.1186/1471-2164-5-99
Sanges, R., Hadzhiev, Y., Gueroult-Bellone, M., Roure, A., Ferg, M., Meola, N., Amore, G., Basu, S., Brown, E.R., De Simone, M., Petrera, F., Licastro, D., Strähle, U., Banfi, S., Lemaire, P., Birney, E., Müller, F., Stupka, E., 2013. Highly conserved elements discovered in vertebrates are present in non-syntenic loci of tunicates, act as enhancers and can be transcribed during development. Nucleic Acids Res. 41, 3600–3618. https://doi.org/10.1093/nar/gkt030
Sanges, R., Kalmar, E., Claudiani, P., D'Amato, M., Muller, F., Stupka, E., 2006. Shuffling of cis-regulatory elements is a pervasive feature of the vertebrate lineage. Genome Biol. 7, R56. https://doi.org/10.1186/gb-2006-7-7-r56
Sawyer, R.H., Knapp, L.W., 2003. Avian skin development and the evolutionary origin of feathers. J. Exp. Zoolog. B Mol. Dev. Evol. 298, 57–72. https://doi.org/10.1002/jez.b.26
Schep, R., Necsulea, A., Rodríguez-Carballo, E., Guerreiro, I., Andrey, G., Nguyen Huynh, T.H., Marcet, V., Zákány, J., Duboule, D., Beccari, L., 2016. Control of Hoxd gene transcription in the mammary bud by hijacking a preexisting regulatory landscape. Proc. Natl. Acad. Sci. U. S. A. 113, E7720–E7729. https://doi.org/10.1073/pnas.1617141113
Schmidt, D., Wilson, M.D., Ballester, B., Schwalie, P.C., Brown, G.D., Marshall, A., Kutter, C., Watt, S., Martinez-Jimenez, C.P., Mackay, S., Talianidis, I., Flicek, P., Odom, D.T., 2010. Five-Vertebrate ChIP-seq Reveals the Evolutionary Dynamics of Transcription Factor Binding. Science 328, 1036–1040. https://doi.org/10.1126/science.1186176
Shao, Z., Zhang, Y., Yuan, G.-C., Orkin, S.H., Waxman, D.J., 2012. MAnorm: a robust model for quantitative comparison of ChIP-Seq data sets. Genome Biol. 13, R16. https://doi.org/10.1186/gb-2012-13-3-r16
Snetkova, V., Ypsilanti, A.R., Akiyama, J.A., Mannion, B.J., Plajzer-Frick, I., Novak, C.S., Harrington, A.N., Pham, Q.T., Kato, M., Zhu, Y., Godoy, J., Meky, E., Hunter, R.D., Shi, M., Kvon, E.Z., Afzal, V., Tran, S., Rubenstein, J.L.R., Visel, A., Pennacchio, L.A., Dickel, D.E., 2021. Ultraconserved enhancer function does not require perfect sequence conservation. Nat. Genet. 53,

521–528. https://doi.org/10.1038/s41588-021-00812-3
Sockanathan, S., Sockanathan, S., 2015. In situ hybridization of chick and mouse embryonic tissue. Protoc. Exch. https://doi.org/10.1038/protex.2015.040
Spitz, F., Furlong, E.E.M., 2012. Transcription factors: from enhancer binding to developmental control. Nat. Rev. Genet. 13, 613–626. https://doi.org/10.1038/nrg3207
Spitz, F., Gonzalez, F., Peichel, C., Vogt, T.F., Duboule, D., Zakany, J., 2001. Large scale transgenic and cluster deletion analysis of the HoxD complex separate an ancestral regulatory module from evolutionary innovations. Genes Dev 15, 2209–14. https://doi.org/10.1101/gad.205701
Torosin, N.S., Anand, A., Golla, T.R., Cao, W., Ellison, C.E., 2020. 3D genome evolution and reorganization in the Drosophila melanogaster species group. PLOS Genet. 16, e1009229. https://doi.org/10.1371/journal.pgen.1009229
Ushiki, A., Zhang, Y., Xiong, C., Zhao, J., Georgakopoulos-Soares, I., Kane, L., Jamieson, K., Bamshad, M.J., Nickerson, D.A., University of Washington Center for Mendelian Genomics, Shen, Y., Lettice, L.A., Silveira-Lucas, E.L., Petit, F., Ahituv, N., 2021. Deletion of CTCF sites in the SHH locus alters enhancer-promoter interactions and leads to acheiropodia. Nat. Commun. 12, 2282. https://doi.org/10.1038/s41467-021-22470-z
Vierstra, J., Rynes, E., Sandstrom, R., Zhang, M., Canfield, T., Hansen, R.S., Stehling-Sun, S., Sabo, P.J., Byron, R., Humbert, R., Thurman, R.E., Johnson, A.K., Vong, S., Lee, K., Bates, D., Neri, F., Diegel, M., Giste, E., Haugen, E., Dunn, D., Wilken, M.S., Josefowicz, S., Samstein, R., Chang, K.-H., Eichler, E.E., De Bruijn, M., Reh, T.A., Skoultchi, A., Rudensky, A., Orkin, S.H., Papayannopoulou, T., Treuting, P.M., Selleri, L., Kaul, R., Groudine, M., Bender, M.A., Stamatoyannopoulos, J.A., 2014. Mouse regulatory DNA landscapes reveal global principles of cis-regulatory evolution. Science 346, 1007–1012. https://doi.org/10.1126/science.1246426
Villar, D., Berthelot, C., Aldridge, S., Rayner, T.F., Lukk, M., Pignatelli, M., Park, T.J., Deaville, R., Erichsen, J.T., Jasinska, A.J., Turner, J.M.A., Bertelsen, M.F., Murchison, E.P., Flicek, P., Odom, D.T., 2015. Enhancer Evolution across 20 Mammalian Species. Cell 160, 554–566. https://doi.org/10.1016/j.cell.2015.01.006
Widelitz, R.B., Chuong, C.M., 1999. Early events in skin appendage formation: induction of epithelial placodes and condensation of dermal mesenchyme. J. Investig. Dermatol. Symp. Proc. Soc. Investig. Dermatol. Inc Eur. Soc. Dermatol. Res. 4, 302–306. https://doi.org/10.1038/sj.jidsp.5640234
Woltering, J.M., Noordermeer, D., Leleu, M., Duboule, D., 2014. Conservation and Divergence of Regulatory Strategies at Hox Loci and the Origin of Tetrapod Digits. PLoS Biol 12, e1001773. https://doi.org/10.1371/journal.pbio.1001773
Wong, E.S., Zheng, D., Tan, S.Z., Bower, N.I., Garside, V., Vanwalleghem, G., Gaiti, F., Scott, E., Hogan, B.M., Kikuchi, K., McGlinn, E., Francois, M., Degnan, B.M., 2020. Deep conservation of the enhancer regulatory code in animals. Science 370. https://doi.org/10.1126/science.aax8137
Wu, P., Hou, L., Plikus, M., Hughes, M., Scehnet, J., Suksaweang, S., Widelitz, R., Jiang, T.-X., Chuong, C.-M., 2004. Evo-Devo of amniote integuments and appendages. Int. J. Dev. Biol. 48, 249–270. https://doi.org/10.1387/ijdb.041825pw
Yakushiji-Kaminatsui, N., Lopez-Delisle, L., Bolt, C.C., Andrey, G., Beccari, L., Duboule, D., 2018. Similarities and differences in the regulation of HoxD genes during chick and mouse limb development. PLoS Biol. 16, e3000004. https://doi.org/10.1371/journal.pbio.3000004
Yu, Z., Jiang, K., Xu, Z., Huang, H., Qian, N., Lu, Z., Chen, D., Di, R., Yuan, T., Du, Z., Xie, W., Lu, X., Li, H., Chai, R., Yang, Y., Zhu, B., Kunieda, T., Wang, F., Chen, T., 2018. Hoxc-Dependent Mesenchymal Niche Heterogeneity Drives Regional Hair Follicle Regeneration. Cell Stem Cell 23, 487-500.e6. https://doi.org/10.1016/j.stem.2018.07.016
Zákány, J., Kmita, M., Alarcon, P., de la Pompa, J.-L., Duboule, D., 2001. Localized and Transient Transcription of Hox Genes Suggests a Link between Patterning and the Segmentation Clock. Cell 106, 207–217. https://doi.org/10.1016/S0092-8674(01)00436-6

Zhang, Y., Liu, T., Meyer, C.A., Eeckhoute, J., Johnson, D.S., Bernstein, B.E., Nusbaum, C., Myers, R.M., Brown, M., Li, W., Liu, X.S., 2008. Model-based analysis of ChIP-Seq (MACS). Genome Biol 9, R137. https://doi.org/10.1186/gb-2008-9-9-r137
Ziebarth, J.D., Bhattacharya, A., Cui, Y., 2012. CTCFBSDB 2.0: a database for CTCF-binding sites and genome organization. Nucleic Acids Res. 41, D188–D194. https://doi.org/10.1093/nar/gks1165

Hintermann et al.
Figure 1

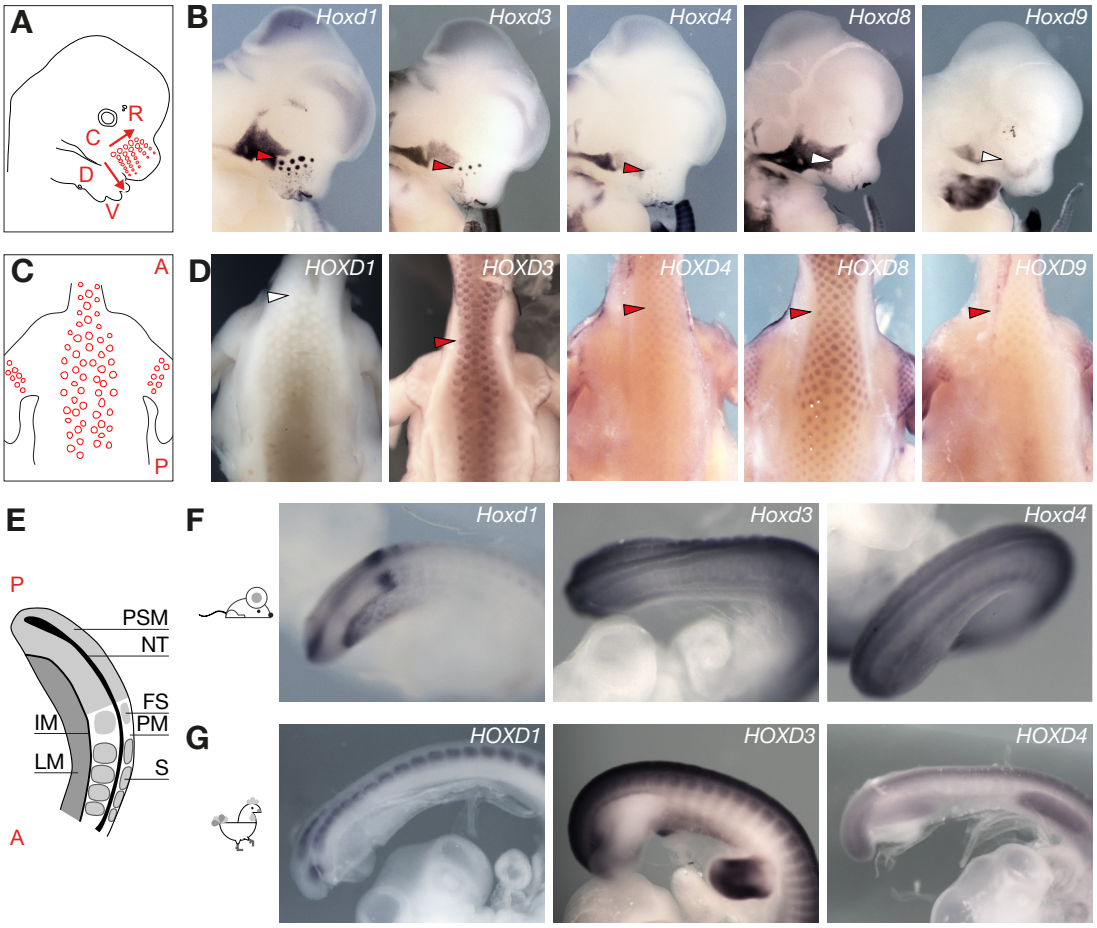

Hintermann et al.
Figure 2

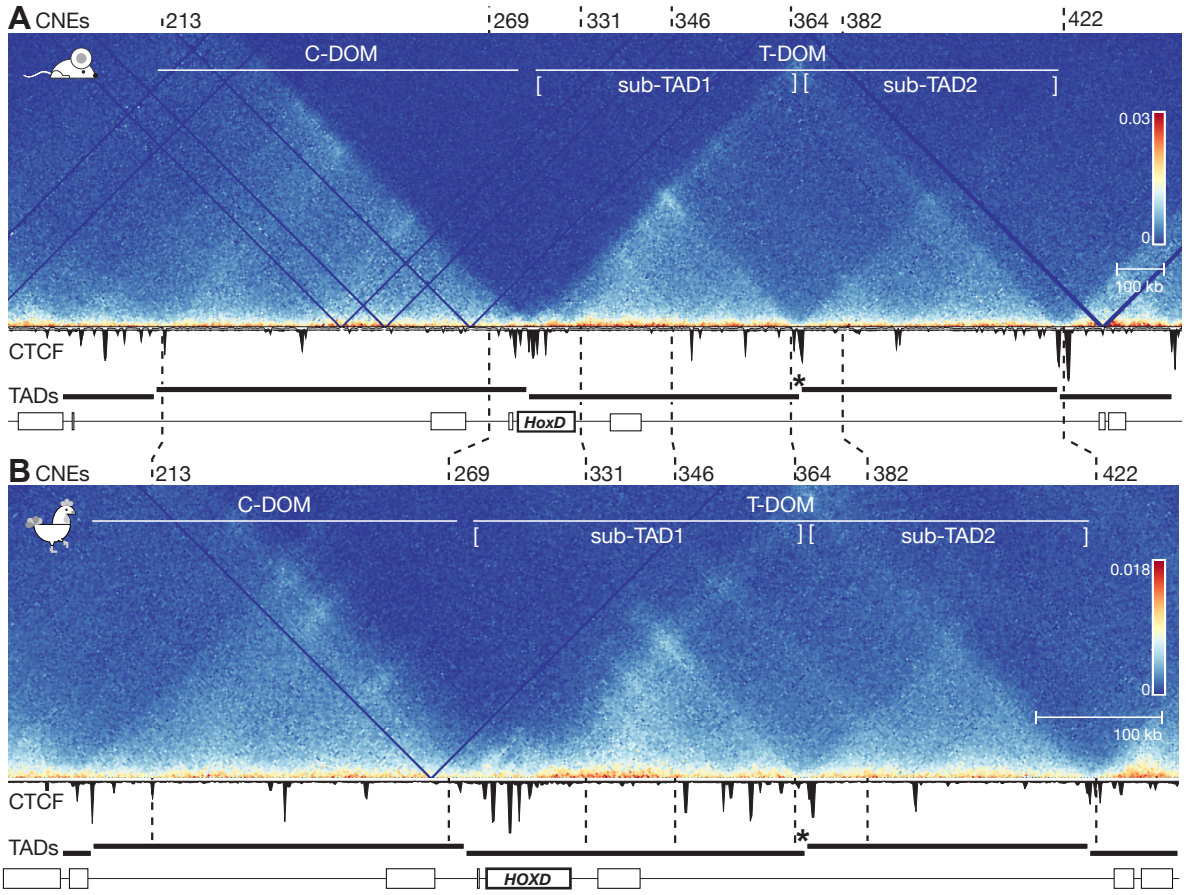

Hintermann et al.
Figure 3

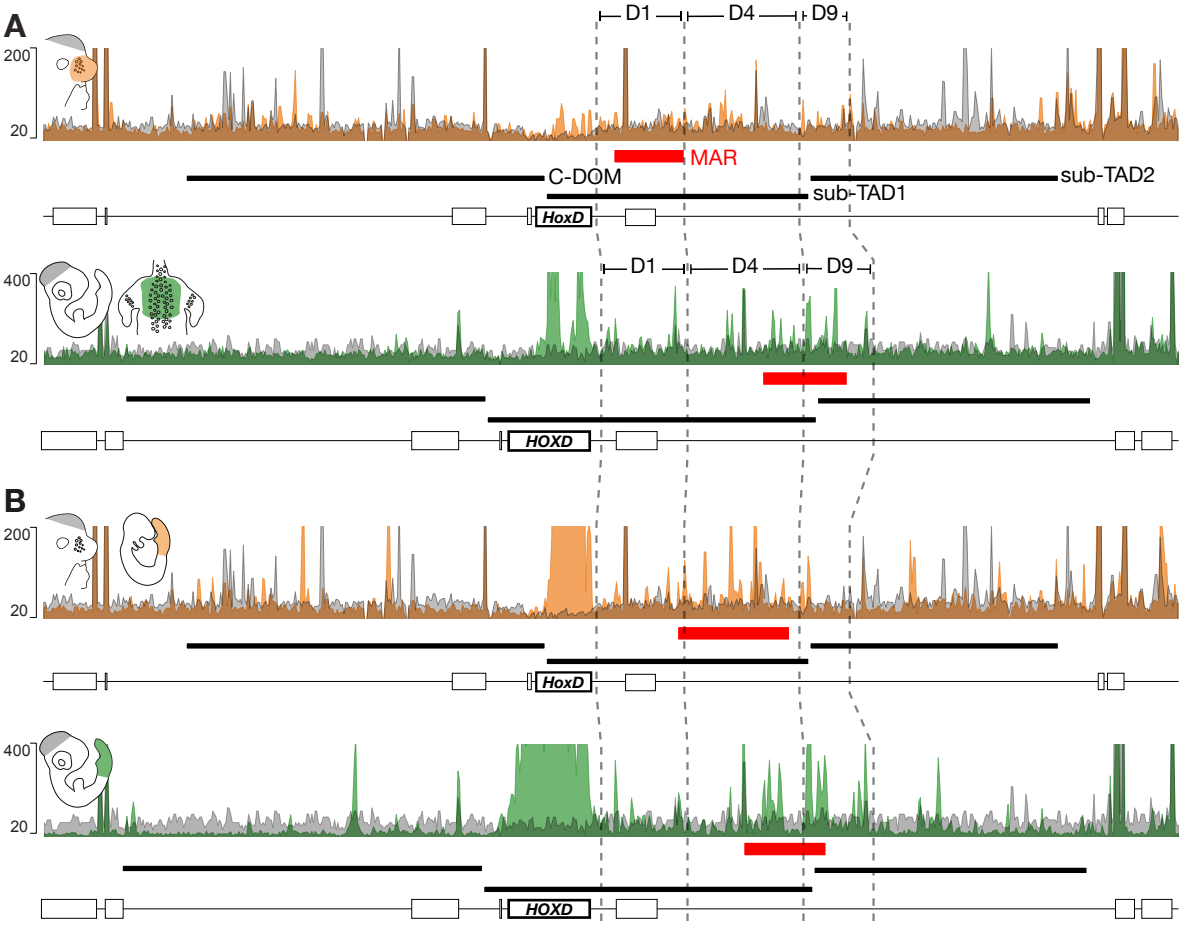

Hintermann et al.
Figure 4

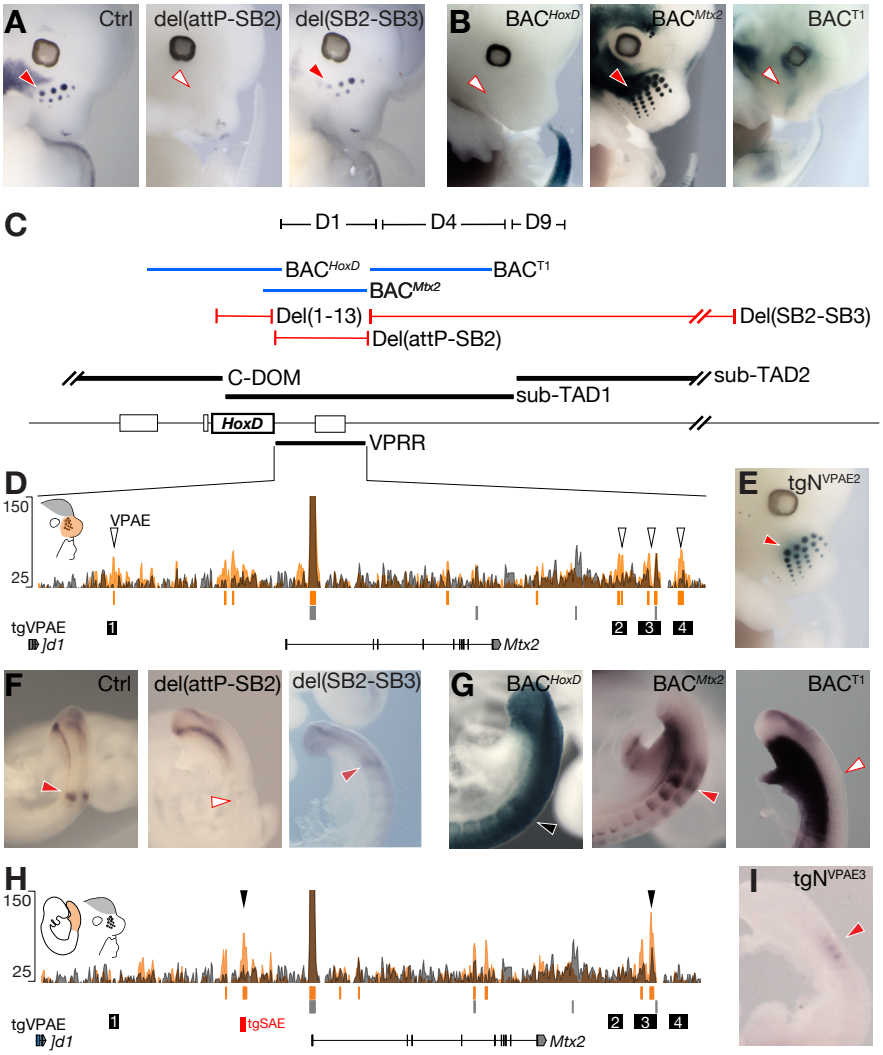

Hintermann et al.
Figure 5

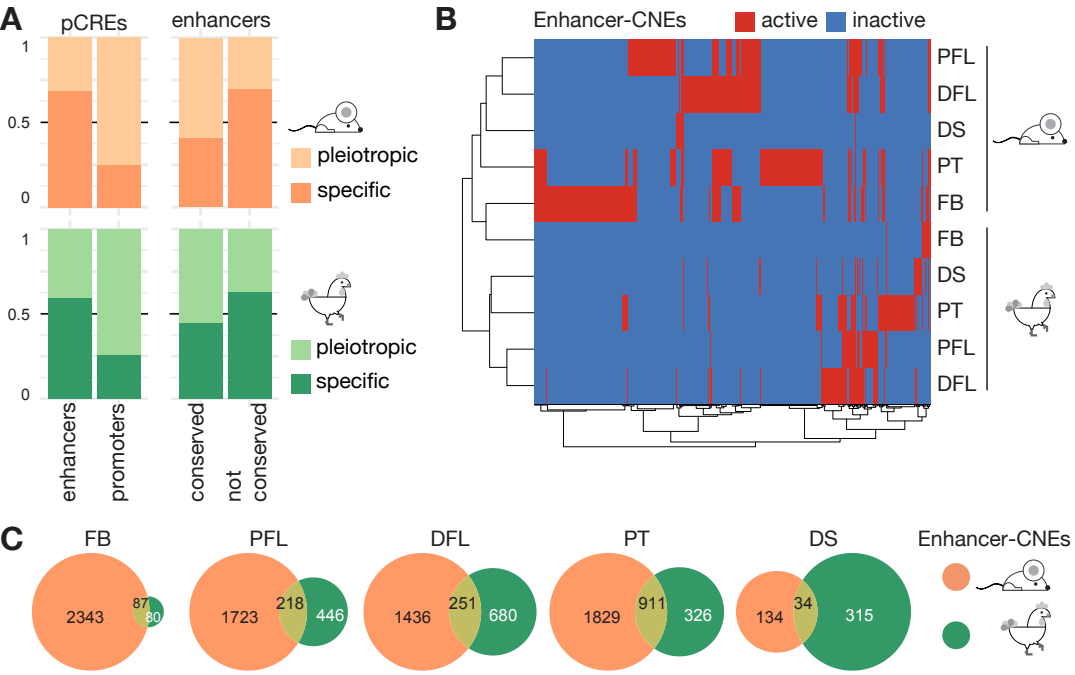

Hintermann et al.
Supplementary Figure S1

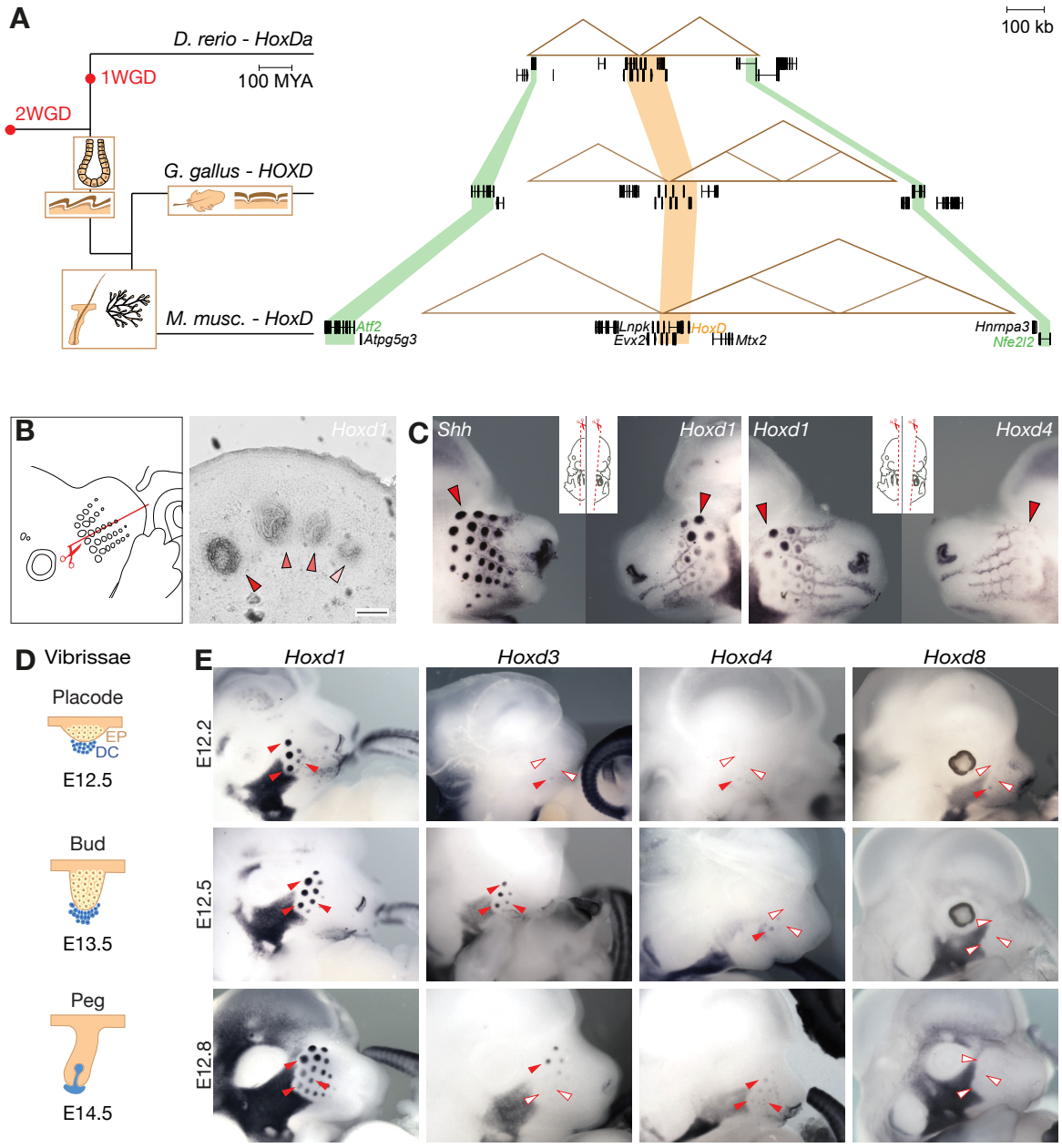

Hintermann et al.
Supplementary Figure S2

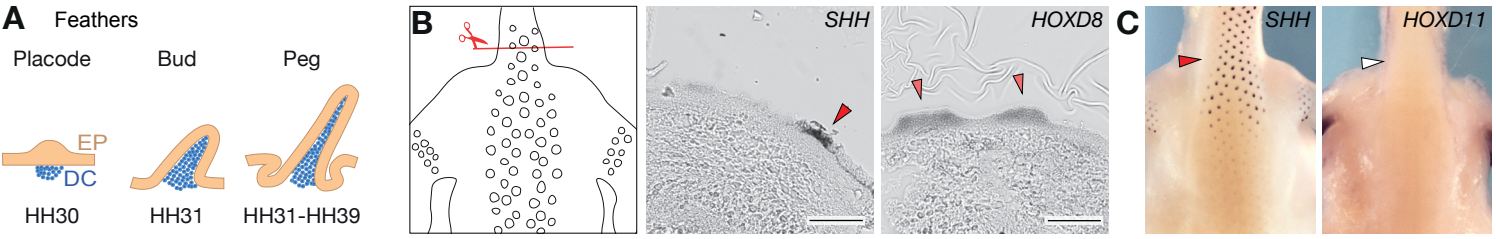

Hintermann et al.
Supplementary Figure S3

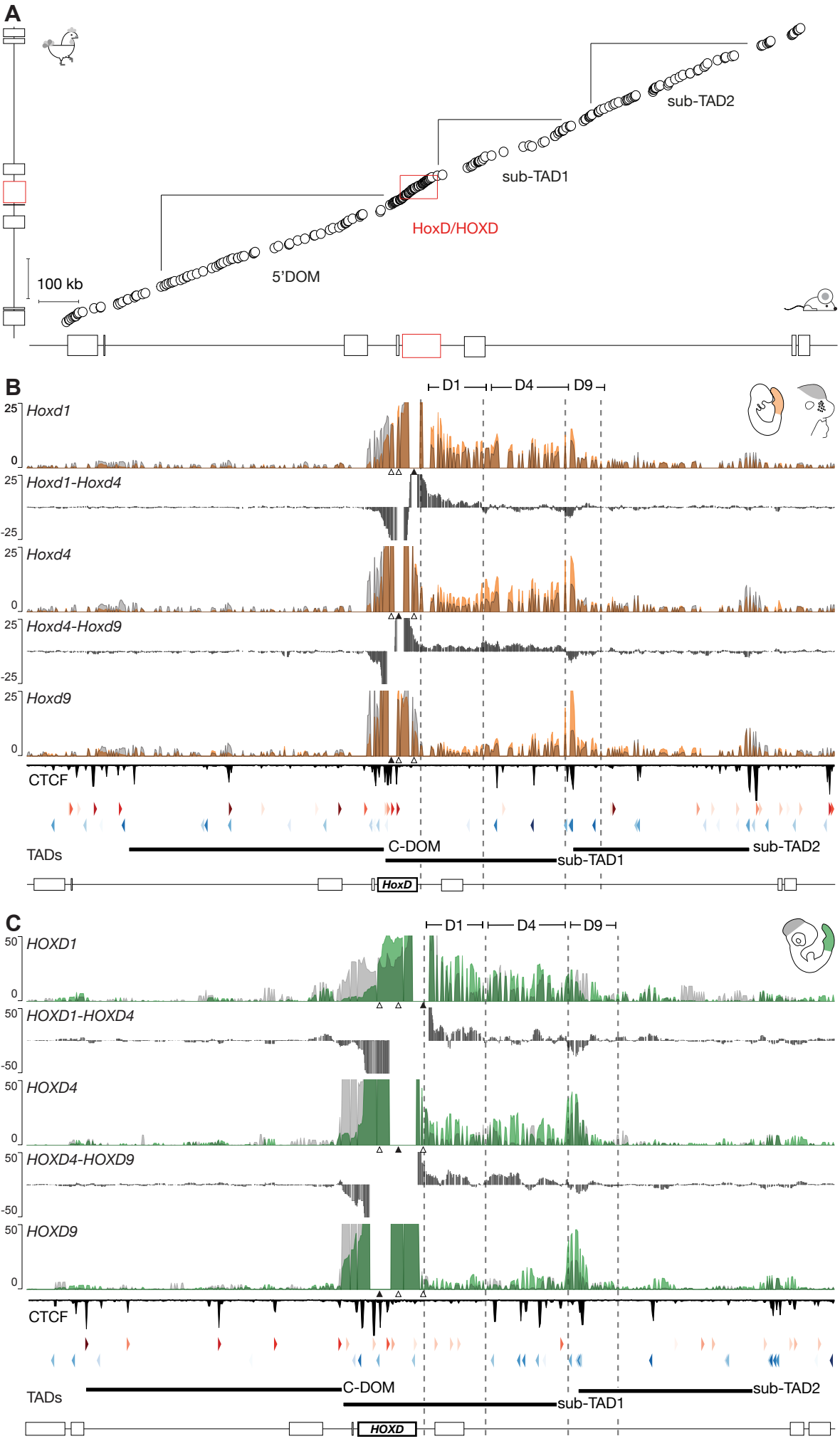

Hintermann et al.
Supplementary Figure S4

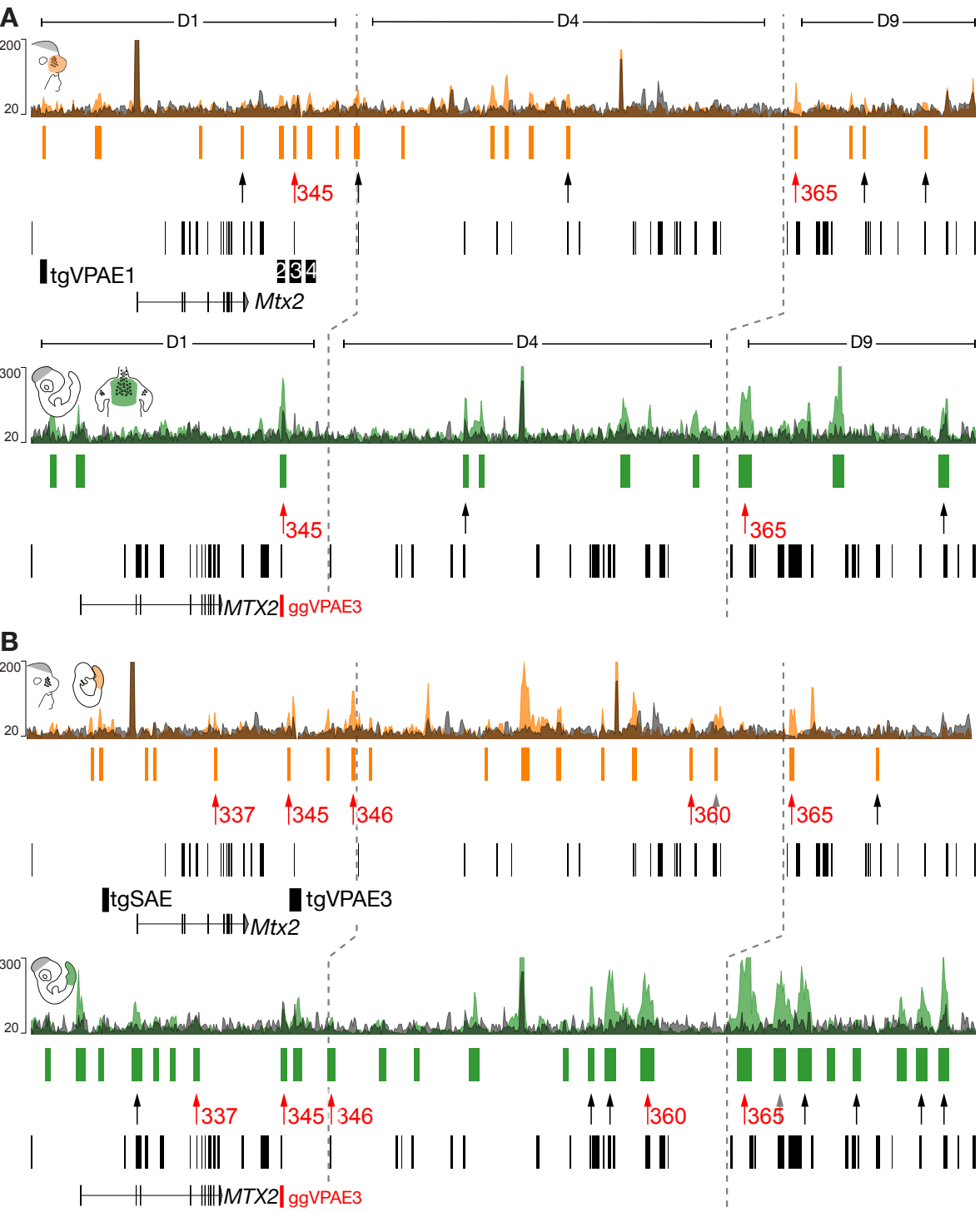

Hintermann et al.
Supplementary Figure S5

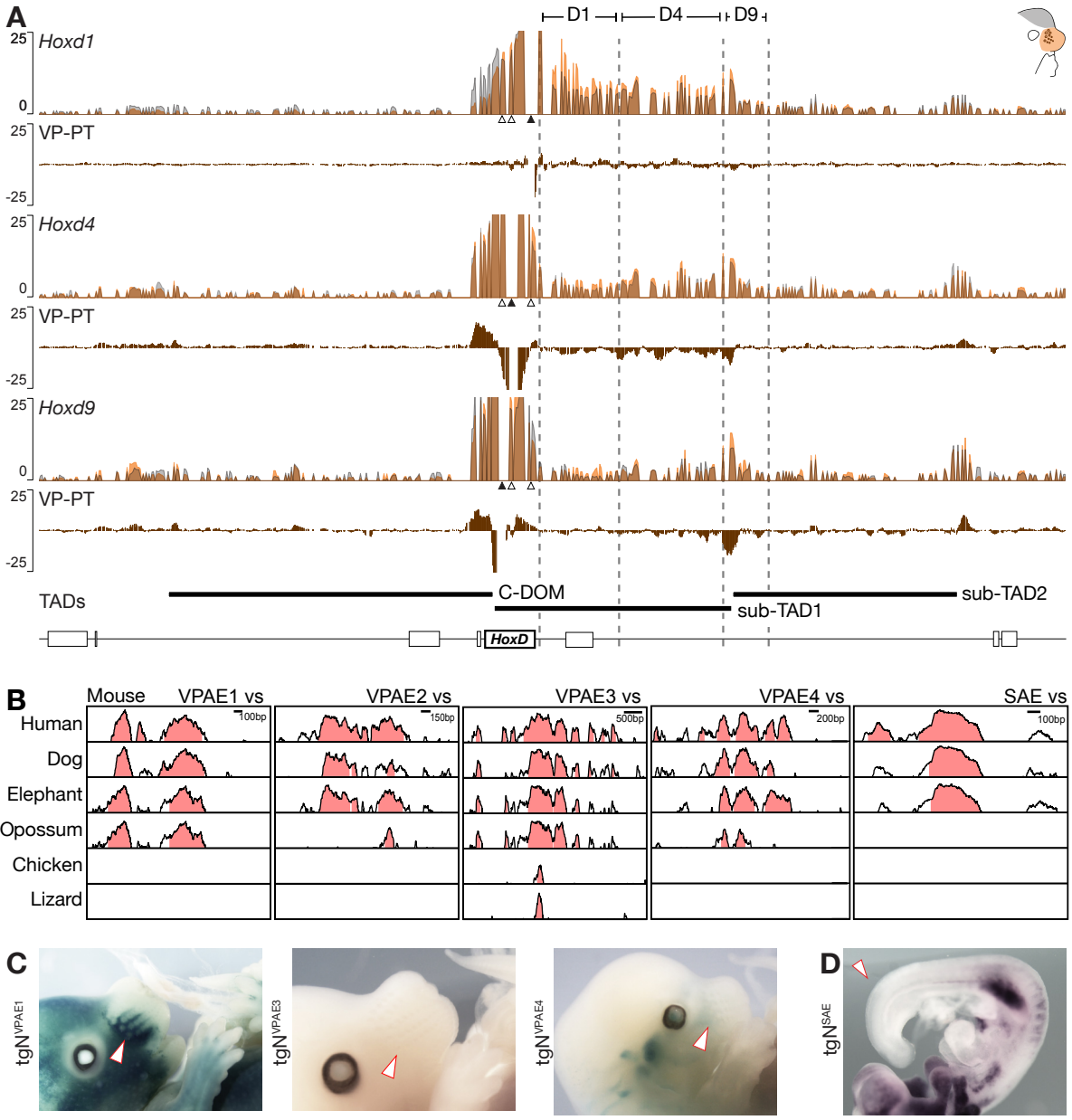
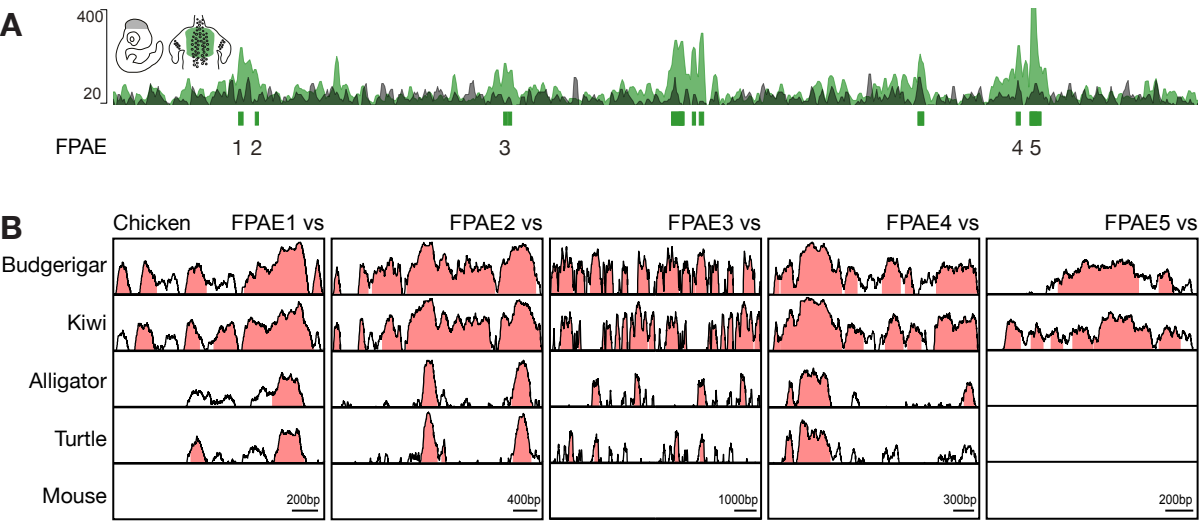
Hintermann et al.
Supplementary Figure S6